Development of Automated Algorithms for Epicardial Adipose Tissue Analysis in Computed Tomography and their Application in Population Based Research

David Molnar

Department of Molecular and Clinical Medicine

Institute of Medicine

Sahlgrenska Academy, University of Gothenburg

UNIVERSITY OF GOTHENBURG

Gothenburg 2024

david.molnar@gu.se

ISBN 978-91-8069-561-9 (PRINT)
ISBN 978-91-8069-562-6 (PDF)

Printed in Borås, Sweden 2024
Printed by Stema Specialtryck AB

”Han befann sig nu i ett tillstånd mellan
fanatism och absolut indifferentism,
det berodde endast på nästa impuls
vad riktning det skulle ta.”

August Strindberg

ABSTRACT

The epicardial adipose tissue (EAT), which surrounds the heart and is separated from other tissues only by the thin layers of the pericardium, has enjoyed intense research for the past decades. Increased inflammatory activity in the EAT in coronary artery disease has, together with associated volumetric expansion of the EAT and changes in its radiodensity supported theories that the EAT might play a role in the pathogenesis of coronary atherosclerosis or mirror its progression better than traditional risk factors. Cardiac computed tomography (CT) has been the most frequently used method for in vivo imaging of the EAT, but reliance on labor-intense manual or semi-automated analyses has limited most studies to small cohorts or incomplete EAT data. Lately, new frontiers have been opened by advances in artificial intelligence-based image analysis.

Within the framework of the current thesis, a fully automated model has been developed and validated in CT images from a total of more than 1,400 individuals. The model's performance is equal to that of manual expert measurements, with the capability to handle: a) anatomical variation in an unselected population b) incomplete images c) high noise levels.

The relationship between EAT and pre-diabetes was investigated in 1,948 individuals, and an automated quality-control algorithm was added to find unsuccessful analyses (< 1%). In the next paper, EAT data was examined in relation to coronary artery calcifications, while in the final paper, its relation to vector electrocardiographic signs of abnormal QRS-T angles reflecting ventricular de-/repolarization was investigated in 5,571 individuals.

Results show that large cohorts can be efficiently analyzed with the model. The co-variation between EAT data and traditional anthropometric and laboratory derived risk factors is substantial and EAT is not superior to these in identifying the presence of coronary artery calcifications or abnormal QRS-T angles in vector electrocardiography indicative of disease.

Keywords: Epicardial adipose tissue, artificial intelligence, automatic analysis, computed tomography, coronary atherosclerosis, pre-diabetes, vector electrocardiography

ISBN 978-91-8069-561-9 (PRINT)
ISBN 978-91-8069-562-6 (PDF)

SAMMANFATTNING PÅ SVENSKA

Det epikardiella fettet (EAT), som omger hjärtat, har varit föremål för intensiv forskning de senaste decennierna. Förhöjd inflammatorisk aktivitet i denna fettvävnad och ett samband med ökade volymer och förändringar i dess röntgentäthet vid kranskärlssjukdom har givit stöd för teorin att EAT kan vara av betydelse för sjukdomsutvecklingen eller spegla dess svårighetsgrad bättre än traditionella riskfaktorer. Icke-invasiv avbildning med skiktröntgenteknik är den metod som använts i störst utsträckning. Hittillsvarande bildanalysmetoder har byggt på manuella eller halvautomatiska mätningar, vilket begränsat de flesta studier till storleken och analysernas omfattning. Nyligen gjorda framsteg inom bildanalys baserad på artificiell intelligens har dock öppnat nya möjligheter. Inom ramen för denna avhandling har en helt automatisk analysmodell med en träffsäkerhet jämförbar med manuella expertmätningar utvecklats, som också klarar av att hantera: a) anatomisk variation i befolkningen, b) ofullständiga bilder, c) höga brusnivåer.

Sambanden mellan EAT och förstadier till åldersdiabetes undersöktes i en kohort om 1948 individer, där en algoritm för automatisk kvalitetskontroll också byggdes in för att filtrera ut misslyckade analyser (<1%). I nästa delarbete undersöktes sambandet mellan EAT och förkalkningar i kranskärlen, medan sambandet mellan EAT och tecken på störd de-/repolarisering i hjärtmuskeln i form av onormala QRS-T vinklar mätta med vektorkardiografi kartlades bland 5571 individer i sista delarbetet.

Resultaten visar att stora kohorter kan undersökas effektivt med modellen men också att EAT samvarierar i betydande grad med kroppsmått och flertalet biokemiska riskmarkörer och inte är överlägset dessa traditionella riskfaktorer när det kommer till att identifiera åderförkalkning i kranskärlen eller onormala vektorkardiografiska QRS-T vinklar tydande på sjukdom.

LIST OF PAPERS

This thesis is based on the following studies, referred to in the text by their Roman numerals:

I. Norlén, A., Alvén, J., Molnar, D., Enqvist, O., Norrlund, R. R., Brandberg, J., Bergstrom, G., & Kahl, F. (2016). Automatic pericardium segmentation and quantification of epicardial fat from computed tomography angiography. *J Med Imaging (Bellingham)*, *3*(3), 34003.

II. Molnar, D., Enqvist, O., Ulén, J., Larsson, M., Brandberg, J., Johnsson Å, A., Björnson, E., Bergström, G., & Hjelmgren, O. (2021). Artificial intelligence based automatic quantification of epicardial adipose tissue suitable for large scale population studies. *Sci Rep*, *11*(1), 23905.

III. Molnar, D., Björnson, E., Larsson, M., Adiels, M., Gummesson, A., Bäckhed, F., Hjelmgren, O., & Bergström, G. (2023). Pre-diabetes is associated with attenuation rather than volume of epicardial adipose tissue on computed tomography. *Scientific Reports*, *13*(1), 1623.

IV. Molnar, D., Björnson, E., Hjelmgren, O., Adiels, M., Bäckhed, F., & Bergström, G. Coronary artery calcifications in relation to epicardial adipose tissue volume and attenuation on cardiac computed tomography in a cohort of 1,945 individuals with various degrees of glucose disorders. *Manuscript.*

V. Molnar, D., Bergfeldt, L., Björnson, E., Hjelmgren, O., Adiels, M. & Bergström, G. Vector electrocardiographic QRS-T angle abnormalities are not correlated to epicardial adipose tissue volume or attenuation on cardiac computed tomography in a population sample of 5.571 individuals. *Manuscript*.

CONTENTS

ABBREVIATIONS

AI	Artificial intelligence
AUC	Area under the curve
BMI	Body mass index
CAC	Coronary artery calcification
CACS	Coronary artery calcium score
CGI	Combined glucose intolerance
CNN	Convolutional neural network
CT	Computed tomography
CCT	Contrast-enhanced computed tomography
DL	Deep learning
EAT	Epicardial adipose tissue
EATA	Epicardial adipose tissue attenuation
EATV	Epicardial adipose tissue volume
ECG	Electrocardiography
FDG	Fluorodeoxyglucose
HU	Hounsfield unit
IFG	Impaired fasting glucose
IGT	Impaired glucose tolerance
IVUS	Intravascular ultrasound
ML	Machine learning

MRI	Magnetic resonance imaging
NCCT	Non-contrast-enhanced computed tomography
NGT	Normal glucose tolerance
PET	Positron emission tomography
ROC	Receiver operator characteristic
SCAPIS	Swedish CArdioPulmonary bioImage Study
T2D	Type-2 diabetes
VATA	Visceral adipose tissue area
VCG	Vector electrocardiography, vectorcardiography

1 INTRODUCTION

1.1 THE EPICARDIAL ADIPOSE TISSUE (EAT)

The epicardial adipose tissue (EAT) is a fatty tissue immediately in contact with and surrounding the myocardium, enclosed by the two layers of the pericardium, which are separated from each other only by a thin layer of fluid[1]. The EAT is considered to be a special type of visceral adipose tissue[2], and as such, differs from the subcutaneous adipose tissue in several key aspects. It has been postulated to function not only as an insulating tissue with regards to the coronary arteries, which are embedded in it, but also to provide warmth and metabolic support to the myocardium, being a reservoir of both energy and rich in brown adipose tissue[3–5]. The discovery of increased inflammatory activity in the EAT in the setting of coronary artery disease has suggested that it also has a possible immunological or endocrine function[6–8]. It is known from anatomical, pathological and imaging studies in vivo, that the EAT has a composition and characteristics, which are not static, but vary with age[2,9], hormonal influences[10], metabolic status[11,12], and the presence of various disease conditions, among which coronary atherosclerosis[7,13–15] and diabetes[16,17] have been the most studied. There seems to be a physiological increase in the EAT volume (EATV) with age, while the relative amount of brown adipose tissue, while obviously varying with the seasonal need for heat generation[18], seems to decrease with age[19]. The attenuation of the EAT (EATA), or its radiodensity on computed tomography (CT), seems to be particularly prone to a certain volatility due to factors of contradictory influence. While aging by itself, due to the relative decrease of brown adipose tissue, as well as a volumetric expansion, seems to reduce the EATA, inflammation and its consequences seem to increase the EATA, at least locally[20–22]. Visceral adiposity, as seen in the metabolic syndrome, or in the context of pre-diabetes, seems to be associated with a decreased EATA[23,24]. Anatomically complex, the heart does not have an even distribution of the EAT, which is significantly more voluminous around the large coronary artery branches, which occupy the coronary grooves separating the atria from the ventricles with respect to superficial anatomy. There is also a relative paucity of EAT over the left ventricle, in comparison to the underlying muscle mass[2,3].

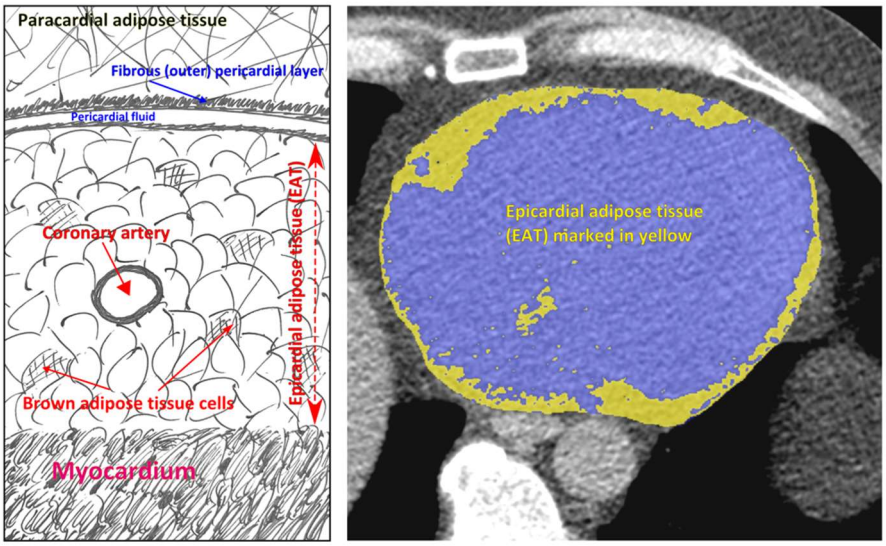

Figure 1. Left pane: Schematic drawing of the epicardial adipose tissue (EAT) and its relation to the myocardium, coronary arteries, pericardium and paracardial adipose tissue. Right pane: A computed tomography image where the pericardium has been automatically segmented and the EAT identified (in yellow). The right coronary artery is visible as an island of blue within the EAT near the upper left corner of the image.

1.2 IMAGING MODALITIES AND IMAGING OF THE EAT WITH CARDIAC COMPUTED TOMOGRAPHY

There are several possible methods available for imaging of the EAT in vivo, among which ultrasound-based measurement of its thickness was the first employed in research on a larger scale. This method has the advantage of being harmless and readily available in most institutions but suffers from severe limitations in that it is highly user- and patient-dependent and delivers only a very restricted amount information[25]. CT soon overtook the position as the most frequently used imaging method with all its advantages including high spatial resolution and reproducibility, partly owing to the development of electrocardiographically gated data acquisition[26–28], and the abundance of information provided, which apart from the EATV delivers inherent information on the EATA. The main limitations are a small, but not negligible exposure to x-rays for the individual examined, and at least until recently, a relatively higher cost[29–31]. Magnetic resonance imaging (MRI) has been used in parallel with the other techniques, with the advantage of a potentially better

qualitative characterization of the EAT, but it has a significantly lower spatial resolution than CT, and is not suitable for the quantification of calcifications, while also being more time consuming, expensive and less available[32,33]. Finally, positron emission tomography (PET) in combination with CT (PET-CT) offers a way to directly investigate the metabolism in the tissues. In cardiac imaging mainly three tracer substances, or sources of positron emission, have been used, ^{18}F-fluorodeoxyglucouse (FDG), ^{18}F-NaF, and ^{15}O-H_2O, the former being in effect a glucose analogue and therefore a reliable estimator of the glucose metabolism, the second a calcium analogue useful for estimating the turnover of calcified tissues, while the latter is water marked with the unstable, positron-emitting form of oxygen and consequently a direct estimator of blood-perfusion in tissues imaged. FDG-PET has been used to assess the glucose metabolism in the EAT, which, if increased is thought to reflect inflammatory activity[34,35], while ^{18}F-NaF-PET has been used to study the calcium turnover in atherosclerotic plaques[36–38], and ^{15}O-H_2O-PET has been utilized to measure myocardial perfusion and its relation to coronary artery disease[39–43]. Unfortunately, PET is relatively expensive, has a comparatively limited availability and suffers from a higher radiation exposure than CT alone due to the added irradiation from the positron-induced secondary gamma-radiation the tissues are subject to[44].

In practice CT has gradually established itself as the chief imaging method, which is also reflected in the multitude of available software applications for the semi-automatic quantification of EAT developed over the past two decades. A majority of studies on the EAT have been performed on non-contrast-enhanced, or native, images, which form the necessary basis for coronary artery calcium scoring (CACS) according to the method originally described by Agatston et al. in 1990[45]. Non-contrast images have the advantage of less contraindications or patient-related complications, and consequently less drop-outs from any cohort, which in contrast-enhanced imaging is seen for various reasons, e.g., allergy to iodine-based contrast agents, or technical difficulties in the injection or contrast-timing. Contrast-enhanced images, however, have a slightly better definition of the pericardium, which renders it easier to track manually, semi-automatically or by any fully automatic model. A possible drawback, on the other hand, is related to the varying degree of contrast enhancement in the EAT itself, obviously depending to large extent on the timing of the image acquisition and the vascularization of the EAT, something which can present difficulties[46] in the interpretation of results.

1.3 DEFINING AND QUANTIFYING THE EAT IN COMPUTED TOMOGRAPHY

An x-ray-based imaging technique, CT is dependent on the transillumination of the examined structures and the detection of the x-rays passing through the object, or in this case, the thorax of the individual examined. The detection has until the advent quite recently of photon-counting detectors been done by means of measuring the capacity of the incident x-rays to excite the detector, usually of scintillator type, generating a signal of light, which in turn is converted by photodiodes to electrical signals dependent on the absorbed energy[47–49]. The attenuation, or loss of energy, as the x-rays pass through the body, is measured in Hounsfield units (HU)[50,51], and, on the Hounsfield scale, by definition, water corresponds to 0 HU, air at room temperature to -1000 HU, and compact bone typically to >1000 HU. The CT images constitute a reconstruction in three dimensions of the attenuation data, which is gathered in 360 degrees around the imaged object either in incremental steps or, in a spiral motion due to a continuous movement of the bed of the scanner in relation to the x-ray tube[52,53]. As a result of the calculations, the image will have a smallest unit, a voxel, which is effectively a pixel but with a volume. The cross-sectional dimension of the voxel in the x-y-plane will depend on the matrix and field of view, which define how many pixels will be calculated in a given area, while the longitudinal dimension, in the z-plane, will depend on detector characteristics such as the number of rows[54,55], their geometry, and, if helical scanning is used, on the incremental movement of the bed, or its pitch. The spatial resolution in any given CT image, which defines the ability to discern small structures, will, on the other hand, be dependent on a multitude of parameters of both the CT scanner, radiation doses used and the characteristics of the organs or body parts which are scanned[56,57]. In physical theory, the wavelength of the radiation used for image generation would set the ultimate resolution limit[58,59], but the practical limits are very far from this. In experimental works with clinically available CT-scanners, a resolution of about 0.3 mm or less, down to about 0.2 mm is attainable[60–63], especially with the newest photon counting detectors[64–66], while voxel dimensions in clinical practice are usually larger. It is implicit, that any single voxel will have only one attenuation value in the reconstructed image, and therefore, adjacent voxels can have different values, if small structures are partly included, or a border between structures of different radiodensity is imaged across neighboring voxels. Adipose tissue is not entirely homogenous in its composition due to the presence of brown adipose tissue not uniformly

interspersed in the white adipose tissue, the presence of blood vessels, and small streaks of denser connective tissue[67]. Adipose tissue in general has empirically been defined as having an attenuation of between -30 and -190 HU, which enables the reader to discriminate with reasonable certainty between it and other soft tissues[68,69]. In a compelling majority, though not all studies of the EAT, this definition of adipose tissue has been used when classifying and quantifying the EAT.

To properly assess the quantity of EAT, the first task is to identify its anatomical border, the pericardium. On CT, this is a thin membrane with an attenuation higher than both the paracardial adipose tissue surrounding it and the EAT inside of it, which is usually not visibly identifiable in its entirety. With due anatomical knowledge and by extrapolating its visible parts, it can be traced with sufficient precision to allow an accurate delineation of the pericardial contour. Once this geometric border of the EAT has been defined, the voxels within the volume of interest can be classified according to their attenuation values. A simple thresholding approach, where any voxels corresponding to the attenuation values of adipose tissue are classified as voxels belonging to the EAT has been the easiest and most widespread in previous research. Some post-processing using mathematical filtering models[70] to eliminate “holes” or “islands” in the volumes has frequently been used, but there is often surprisingly little referencing to the exact ways of calculating the EATV in publications.

1.4 TOWARDS FULLY AUTOMATED EAT MEASUREMENTS

Manual tracing of the pericardium can be very time-consuming if done thoroughly and with high precision, especially if an image stack consists of many thin slices, which is usually the case in contrast-enhanced CT examinations. Semi-automatic tracing of the pericardium has been widely used in research to speed up and simplify the delineation of the pericardium[71–76]. The interpolations require varying degree of manual correction, and although semi-automatic methods offer some relief[77], time constraints still limit the analysis of large datasets, unless precision is sacrificed. With the rapid evolution in artificial intelligence and specifically in automated image interpretation taking place in other fields over the last decade[78–82], projects aspiring to achieve greater automation have been launched in increasing numbers. The first successful attempts[83–89] employed multi-atlas-based

methods[90], where a reference library of shapes and other image characteristics is created, and which is later used to present templates for the model, which give input in the decision tree. Usually some components of machine-learning[91,92] are incorporated into the models at some stage. An obvious advantage of multi-atlas-based segmentation, if the library of reference cases is large, is that it reduces very substantial errors, or outliers, in the identification of structures, since the limits of the most extreme parameters is defined by the reference cases. Among drawbacks are low computational efficiency, and a heavy reliance on previously acquired and input data into the library, with little plasticity in the decisions made. Towards the end of the previous decade, it was increasingly clear, that methods based on convolutional neural networks (CNN)[93,94] had the potential to be more efficient in terms of performance and training. Among advantages of a CNN-based approach we find high computational efficiency, with fast or very fast analyses, great versatility in applicability, with relatively lower demands on the quality of training data, given that successful training can be made even using partial data, and training can be enhanced with various mathematical processing techniques. Obviously, there is a price to these features, and that is mainly the requirement for large or very large datasets to be made available for the training until sufficient performance levels have been reached. On the other hand, data which has been manually quality checked, can be refed to the model as training data, incrementally improving performance. One of the first reports of a CNN-based model successfully applied to quantify EAT in a larger dataset was published by Commandeur et al. in 2018[95]. The model didn't however analyze the entire EATV, but omitted the most inferior part of the volume, which is also the most difficult to delineate, due to the close anatomical relationship with the diaphragm and the sub-diaphragmatic organs of the abdomen. Since then, several publications have forwarded or tested various models based on similar techniques[96–98], the most recent[99] being tested in a cohort of 3,720 individuals.

1.5 THE EAT IN RELATION TO CORONARY ATHEROSCLEROSIS

Coronary atherosclerosis is typically hallmarked by the presence of calcifications in the arterial wall[100–104]. These findings have been extensively researched and reported. With the advent of intravascular ultrasound and optical coherence tomography[105–108], as well as modern CT imaging, the disease process leading to calcifications has become better characterized in vivo, and there is mounting evidence that coronary plaques can have various

degree of lipid content and calcification is not always present[109–117]. Historically, an intriguing negative finding has been the absence of description of coronary atherosclerotic lesions in segments of the coronary arteries which, as part of the normal anatomical variation, have an intramuscular course and are not exposed directly to any neighboring EAT[118]. The discovery of increased inflammatory activity in the EAT[6] in patients undergoing heart surgery for coronary artery stenosis pivoted the field into instant fame and it has been hypothesized that the EAT might very well be directly involved in the regulation of inflammation and further, in the pathogenesis of atherosclerosis[119,120]. These biochemical findings, as well as the pathological findings derived from microscopical studies, were soon followed by various attempts to analyze the EAT in vivo in both cross-sectional and longitudinal studies focusing on its relationship with either outcome measures, such as the incidence of cardiovascular events[13,24,99,121–125], or traditional risk factors[13,126,127] known to have a significant relationship to outcome measures. Aside from some contradictory evidence presented by a few small studies[128,129], the majority of studies seem to have in common, that there are differences in EATV or findings in the EAT, which can be linked to either outcome measures or risk factors[15,130]. The spread in results, both with regards to the strength of measured associations and the plain EATV values themselves is substantial, the latter spanning 78.5-159 ml in some of the key studies (**Table 1**). Gradually, a notion has evolved, that EATV might be counted as a risk factor by itself, and it has even been advocated that EATV could contain more precise information on the risk of cardiovascular events than other established risk factors. An obvious problem in the literature is a lack of standardized measurements, with few studies applying similar criteria for the definition of EATV, its delimitation, and even fewer studies taking into account, or at least clearly stating how incomplete images or noisy images were treated. Attempts have been made to try to diversify analyses into including also EATA data and it has been suggested that a local increase in EATA around known lesions could mirror increased inflammatory activity, findings largely based on studies with intravascular ultrasound (IVUS)[21,131]. IVUS is a very potent method of characterizing the morphological features of the coronary arterial wall and has high reported sensitivity and specificity for the detection of both soft and calcified plaques[132–136]. Changes in perivascular EATA have been linked to the presence of what on CT subsequently has been characterized as high-risk plaques[22,137,138]. Investigations of EATA in a more general way have produced more ambiguous results, however, with less immediate implications. In a few studies[23,24,139,140] a generally decreased EATA was associated with cardiovascular events and/or traditional risk factors. Among the latter,

disorders of glucose metabolism including the metabolic syndrome and pre-diabetic states are especially interesting and provide a possible logical bridge between EATA and coronary atherosclerosis.

***Table 1**. A survey of studies on EAT in relation to coronary atherosclerosis or in the general population, which have made important contributions to the state of knowledge or technical development in the field. The studies are in chronological order from the top. The number of participants is denoted with "n". NCCT refers to non-contrast-enhanced computed tomography, CCT refers to contrast-enhanced computed tomography.*

Authors	Year	Study population (total n)	EATV (ml)	Method
Ding et al.[125]	2009	MESA (1,119)	82 [weighted average]	NCCT, semi-automatic
Mahabadi et al.[73]	2013	Heinz-Nixdorf (4,093)	85.9 [IQR 59.5]	NCCT, manual
Britton et al.[75]	2013	Framingham (3,086)	111 [68-154]	NCCT, semi-automatic
Forouzandeh et al.[74]	2013	Prospective, symptomatic (760)	127 [66-188]	NCCT, semi-automatic
Kunita et al.[76]	2014	Screening, risk population (722)	107 [79.9-138.2]	NCCT, semi-automatic
Commandeur et al.[141]	2019	EISNER etc., multi-center (776)	86.8 [64.2-119.6]	NCCT, automatic
Marwan et al.[142]	2019	Clinical cases (227)	159 [83-235]	NCCT vs. CCT, semi-automatic
Mancio et al.[143]	2020	EPICHEART, aortic stenosis (574)	109.7 [53.8-165.6]	NCCT, semi-automatic
Milanese et al.[144]	2020	ALTER-BIO (1,344)	90.5 [11.3-442.2]	CCT, semi-automatic
Eisenberg et al.[122]	2020	EISNER (2,068)	78.5 [55.9-106.0]	NCCT, automatic

1.6 THE EAT IN RELATION TO PRE-DIABETES AND TYPE-2-DIABETES

As a visceral fat depot, EAT shares some characteristics with the abdominal visceral adipose tissue, while it also exhibits some differences, especially with regards to its beige characteristics[19,67,145], or amount of brown adipose tissue, and the immediate contact with the myocardium[146,147]. It seems, that in a state of dietary caloric abundance, EAT expands in parallel with the abdominal visceral adipose tissue[72,148–152]. The question is rather: how are these changes related, and is there a difference in the dynamics of changes? Obesity is one of the main, if not the key risk factor for the development of type-2-diabetes (T2D)[153]. Gradual changes have been described in the pathogenesis of T2D, where states of impaired glucose homeostasis precede the fully developed clinical disease[154–159]. These states of pre-diabetes[160–162] have been divided into:

impaired fasting glucose (IFG), impaired glucose tolerance (IGT), and combined glucose intolerance (CGI). CGI represents the most advanced pre-diabetic stage, immediately preceding T2D, where fasting glucose levels are elevated and oral glucose tolerance testing is pathological. CGI progresses to T2D in a majority of cases[162,163], while both IFG, which is thought to represent an early stage mainly linked to abnormal hepatic regulation, and IGT, which is mainly linked to reduced peripheral insulin sensitivity[164,165], can be reverted "spontaneously" under favorable conditions[166–170]. The EATV has been shown to be significantly increased in T2D and CGI[16,17,171]. At the same time, we know that the EATV increases with age, and that both these conditions tend to occur in an older age group. The amount of contribution to the increase in EATV from the metabolic derangements seen in pre-diabetes[171–173] and T2D[23,174–176] is difficult to gauge from existing studies, since most of them derive their data from small or heterogenous cohorts (**Table 2**). In obesity, the volumetric expansion of adipose tissue seems to be driven mainly by hypertrophy of the lipocytes[177,178], which increase their content of lipids. As a consequence, EATA shows a very strong inverse correlation with EATV, being lower with increasing EATV. The kinetics of changes is not fully clarified, and some data suggest, that a relatively larger than expected decrease of EATA can be seen in early pre-diabetes[179]. Whether or not this might indicate a propensity of the EAT to accumulate triglycerides and other low-density lipids in order to compensate for the dysregulated lipid metabolism in states of pre-diabetes[180–183], remains to be elucidated. From a technical point of view, however, the precision in EATA measurements is by default lower than for EATV, with a small range, in which measured values are found, and several potential interfering factors, among which streak artifacts from calcifications in the coronary arteries is of obvious relevance. It is worth mentioning, that only minor differences in EATA between groups have been found in cohort studies, when measuring at whole-heart level[11,122,184,185], and it is realistic to retain some skepticism to conclusions made.

***Table 2**. A survey of studies on EAT in pre-diabetes and type-2 diabetes, which have investigated important cohorts and/or have made important contributions to the technical development in the field. The studies are in inverse chronological order from the top. The number of participants is denoted with "n".*

Authors	Year	Study population (total n)	Groups	n	EATV (ml)	EATA (HU)	Method
Molnar et al.[179]	2023	IGT (1,948)	T2D	73	146.6 [IQR 63.0]	-72 [IQR 7.5]	NCCT, automatic
			CGI	128	134.6 [IQR 65.3]	-71 [IQR 6.0]	
			IGT	321	112.2 [IQR 62.8]	-71 [IQR 6.0]	
			IFG	414	114.7 [IQR 56.0]	-69 [IQR 6.0]	
			NGT	1,012	104.9 [IQR 53.4]	-69 [IQR 8.0]	
Lin et al.[24]	2021	EISNER (2,068)	MetS+	280	114.1 [90.7-147.8]	-76.9±4.6	NCCT, automatic
			MetS-	1,788	73.7 [53.7-98.7]	-73.4±4.6	
Wang et al.[171]	2019	Shanghai, cohort study (668)	NFG	468	117.34 [82.67-167.19]		NCCT, manual
			IFG/IGT	83	173.21 [139.67-219.53]		
			T2D	117	190.64 [138.33-244.82]		
Milanese et al.[23]	2018	Parma, retrospective (1,379)	T2D+	338	112.87 [IQR 68.07]	-80.78±6.06	CCT, semi-automatic
			T2D-	1,041	82.62 [IQR 62.17]	-78.19±5.27	
Groves et al.[176]	2014	California (362)	T2D+	92	118.6 [75.6-161.6]		CCT, manual
			T2D-	270	70.0 [26-114]		
Yang et al.[172]	2013	Taiwan (562)	NGT	357	68.2 [42.7-93.7]		NCCT, manual
			Pre-T2D	155	86.8 [59.9-113.7]		
			T2D+	50	91 [66.9-115.1]		
Versteylen[173]	2012	Utrecht (410)	T2D+	83	98 [57-139]		CCT, manual
			IFG	118	92 [53-131]		
			NFG	209	75 [41-109]		
Wang et al.[174]	2009	Taiwan, case-control study (127)	T2D+	49	166.1 [105.5-226.7]		NCCT, manual
			T2D-	78	123.4 [81.6-165.2]		

T2D=type-2 diabetes, CGI=combined glucose intolerance, IGT=impaired glucose tolerance, IFG=impaired fasting glucose, NGT=normal glucose tolerance, MetS=metabolic syndrome, NFG=normal fasting glucose, pre-T2D=pre-diabetes, EATV=epicardial adipose tissue volume, EATA=epicardial adipose tissue attenuation, NCCT=non-contrast computed tomography, CCT=contrast computed tomography

1.7 THE EAT IN RELATION TO CARDIAC ELECTROPHYSIOLOGICAL CHANGES

The main consequences of coronary atherosclerosis in terms of morbidity and mortality relate to the effects on the myocardium. Myocardial infarction represents the most obvious irreversible effect of insufficient blood flow through the coronary arteries. The spectrum of manifestations is very broad,

ranging from the myocardial damage in microvascular disease to the transmural infarctions affecting an entire vascular territory, leaving no functioning myocardium in the actual area[186]. Electrocardiography (ECG) was the first method capable of visualizing the electrophysiological activity of the heart muscle[187] and the changes in various diseases afflicting the myocardium in a broader sense, including its electroconductive cells. Changes detectable with ECG are not exclusive to, but mainly linked to processes affecting the left ventricle, since it has the largest muscle mass by far, and contributes to the overall electrical activity proportionally. Over the course of the last century, the technique of ECG-registration has been refined, and vector electrocardiography, or vectorcardiography (VCG), has emerged as one of the special applications, with an increased sensitivity for de-/repolarization disorders[188,189]. It is thought that even small changes in the myocardium, be it from microvascular disease, the effects of hypertension, or mere aging, can affect the QRS-T angles of the left ventricle[190–192], which is one of the key features which can be calculated from the VCG[193]. There is some evidence, that the presence of abnormal QRS-T angles increases the risk of sudden cardiac death[193,194], a condition of which ventricular arrhythmias, typically ventricular fibrillation, are a leading cause[195,196]. It is known that coronary atherosclerosis is a risk factor for sudden cardiac death[197], but with respect to the proportion of the risk increase among individuals with abnormal QRS-T angles, which can be accounted for by coronary atherosclerosis, the picture is less clear. Seemingly, abnormal QRS-T angles are associated with some traditional risk factors for cardiovascular disease such as male sex, hypertension, and diabetes[193,198], but the EAT was not among the parameters investigated. There are reports, which indicate that increased amounts of EAT are associated with atrial fibrillation[199–201], a condition primarily defined by its electrophysiological abnormity. Only indirect, circumstantial evidence exists, that might link the EAT to QRS-T angle aberrations on VCG. Here, we find studies pointing to increased inflammation in the EAT in coronary atherosclerosis[20,120,146,202], the association between increased EATV and the presence of coronary atherosclerosis, either measured as CACS or in the form of cardiac events[14,15], the association with changes in EATA reported in conjunction with the presence of atherosclerotic plaques[21,22,203], and finally, the association between changes in EATV[16,17] and EATA[23] in pre-diabetes and T2D. To successfully sort out the complexly interrelated risk factors and their relative influence, large cohorts with high-quality data need to be studied.

2 AIMS OF THE THESIS

The overarching aim has been to develop a model suitable for fully automated EAT analysis in large-scale population studies and, as part of the validation and testing procedures, to explore CT image data available from two fairly large cohorts.

The specific aims of the included papers are listed below.

2.1 PAPER I

To

1. Develop a method for precise and reproducible manual segmentation of the pericardium.
2. Use current state-of-the-art techniques, employing multi-atlas-based automatic segmentations to measure the EATV in a small number of test cases.
3. Evaluate the results as a proof of concept for a) the manual generation of ground truth, and b) the feasibility of fully automatic segmentation.

2.2 PAPER II

To

1. Use the experiences gained from Paper I to generate training data for a new model employing a CNN-based approach for measuring EATV and EATA.
2. Develop the model into a fully automatic one capable of handling: a) anatomical variations in the general population, b) images which are incompletely representing the heart, c) images with varying levels of noise.
3. Validate the model in a cohort representative of the general population of age 50-64.
4. Relate EAT data to previously published EAT data in the literature.
5. Relate EAT data to some key anthropometric and laboratory data considered to be cardiovascular risk factors.

2.3 PAPER III

To

1. Test the fully automatic model in a cohort including individuals with normal glucose metabolism, pre-diabetes and T2D.
2. Improve the model by incorporating and validating an automatic quality-checking algorithm to find potentially flawed analyses.
3. Relate EAT data to the various glucose groups represented in the material.
4. Relate the findings to findings previously described in the literature.

2.4 PAPER IV

To

1. Analyze data from the cohort used in paper III with regards to the presence of coronary artery calcifications and CACS.
2. Test the hypothesis, that increased EATV and decreased EATA are significantly associated with the presence of coronary artery calcifications and to test the independence of the association in relation to co-variates among anthropometric and laboratory based cardiovascular risk factors.
3. Explore the importance of various established cardiovascular risk factors in relation to EAT data in explaining the presence of coronary artery calcifications.

2.5 PAPER V

To

1. Analyze a larger sub-cohort of the SCAPIS-study with regards to EAT data and the presence of abnormal QRS-T angles on VCG.
2. Test the hypothesis, that increased EATV and decreased EATA are significantly associated with abnormal QRS-T angles and to test the independence of the association in relation to co-variates among anthropometric and laboratory based cardiovascular risk factors.
3. Explore the importance of various established cardiovascular risk factors in relation to EAT data in explaining the presence of abnormal QRS-T angles.

3 METHODOLOGICAL CONSIDERATIONS

3.1 COMPUTED TOMOGRAPHY IMAGES

Substantial variation can be expected in image quality depending on the CT-scanner, scan-protocol, and image reconstruction parameters used[204–207]. Apart from these, machine- and setting-specific factors, image quality is known to be influenced by radiographer-related issues such as patient-positioning and the choice of a proper volume to be scanned as well as patient-related issues such as the bodily characteristics of the examined individual, any possible implants which could generate artifacts, and cooperation with regards to, e.g., holding the breath and not moving during scanning.

In large-scale population studies enrolling healthy individuals, where the only reason for being subjected to a CT examination is scientific, requirements for adhering to the lowest possible radiation dose regimen are much tougher relative to what is the case in clinically motivated examinations, and accordingly, inherent noise levels, as they are inversely proportional to the radiation dose, are expected to be substantially increased[208]. The possibilities to re-examine an individual, if image quality is not the desired, is also virtually non-existent for the same reasons, and a larger proportion of images can be expected to be incomplete with regards to the object or region of interest. From a purely technical point of view, there are two reasons for incomplete representation of the volume to be imaged: handling errors from the radiographer misaligning the “box” which delimits the scan volume, and undesired movements including unsuccessful breath holding by the individual undergoing the scan. In a study recruiting only healthy individuals, cooperation would presumably be high, and most cases of incomplete image material can be inferred to be caused by handling errors by the radiographer. In the case of the heart, which is by itself a moving organ, further challenges are presented to the radiographer by the changes in position and orientation when the diaphragm moves with respiration. Moreover, the inferior boundaries of the heart can be difficult to define properly on the survey images taken ahead of the CT scan. The superior limit of the heart can be quite difficult to decide on, unless a clear-cut definition is given a priori, but if one is intent on imaging the entire pericardium, the scanning volume must include a substantial part of the aorta, usually at least past the level of the bifurcation of the pulmonary truncus.

The inclusion of the superior pericardial recesses wrapping around the great vessels, is however of negligible importance, when it comes to analysis of the EAT, since there is virtually no EAT around the vessels, once one has reached the level, where they become tubular.

Images from the pilot-study of the SCAPIS[209], a large population study eventually comprising around 30,000 individuals, were accessible from start for the present thesis. From the pilot-study both non-contrast-enhanced (n=1111) and contrast-enhanced images (n=980) were available for almost all the study participants, acquired on the same occasion. The non-contrast-enhanced images serve primarily the purpose of calcium scoring, while the contrast-enhanced images represent a coronary angiogram. It was clear from the beginning of the thesis project, from the initial visual evaluation, that noise levels were indeed higher than in the typical clinical CT examination, be it with or without contrast, and that the variation in noise-levels was quite dramatic depending on the anatomical conditions given, with the images of some of the individuals suffering from extensive noise-induced artifacts.

3.2 OPTIMIZED MANUAL MEASUREMENTS AND GROUND TRUTH

The contrast-enhanced CT images are available with thinner “slices”, i.e., a voxel size with less extension in the z-axis, and the pericardium is also easier to visualize, since it shows a non-negligible contrast enhancement. For these reasons, they were chosen for the first paper. Testing and optimization experiments soon revealed that manual segmentation, i.e., the “drawing” or annotation of the pericardium, was difficult near the extremes, where the pericardium is almost tangential to the plane of the image slice. Since the thin slices of the contrast-enhanced images enabled segmentation in the three orthogonal planes, it was decided, that the segmentation would be performed sequentially in the axial (x-y), coronal (x-z), and sagittal (y-z) planes, i.e., three times for every individual. Every tenth slice was segmented, which was sufficient in order to generate a smooth pericardial contour when interpolated, since voxel “thickness” was merely 0.3 mm. We could clearly see that the precision in the segmentation, measured as the discrepancy between the segmentation volumes in the three planes, was the greatest inferiorly, anteriorly, and posteriorly. Superiorly, the differences were less conspicuous in absolute volume, given the anatomical shape of the pericardium. It was obvious, that some amount of interpolation was necessary, where the

pericardial contour was not readily identifiable, and that this interpolation had to be made based on anatomical knowledge, neighboring slices or areas, and some "educated guessing", where the principle of the shortest and least tortuous course of the pericardium being true was usually observed. When the segmentations in the three planes were pooled to one volume, the differences, as a lack of overlap, were strikingly typical, and confirmed in essence, that the method for interpolation was feasible. In order to generate a ground truth, which would take into account the fortes and weaknesses of the segmentations in each plane, a mathematical weighting procedure was devised, by which the true contour was decided, giving the least weight to the segmentation data from the tangential plane. It deserves mentioning, that the amount of manual work which this kind of precision demands, is way beyond what would be practically achievable in any study of size: each examination was segmented in around 3 x 40-50 slices, drawing a Bézier curve[210] with between around 10 and 50 points in each slice. For the sake of reproducibility testing, a second expert independently repeated the segmentations according to the exact same procedure. All in all, 30 complete sets of segmentations were generated, of examinations which had been randomly selected in proportions as to represent both sexes equally, while also covering the various strata of BMI found in the material. The inter-reader agreement was in line with levels reported in the literature, and as expected, the differences were concentrated to the difficult areas tangential to the heart. A library of reference images, or of "ground truth" of the highest possible quality had been produced, which would now enable us to test the hypothesis, that fully automated EAT-analysis is possible in images from the SCAPIS with a precision comparable to manual expert analysis.

3.3 A MULTI-ATLAS-BASED METHOD FOR FULLY AUTOMATED EAT ANALYSIS

Around the time of the initiation of the thesis work, various multi-atlas-based strategies were the most successful in terms of accuracy and overall performance. Several publications had presented quite impressive results[83,86,87], either employing intensity-based registration and majority voting, or intensity-based registration and prior co-registration of atlases later filtered by a "Difference of Gaussians" approach to find the best fit. Decision was made on a model largely following the example of Ding et al.[86], with the main difference in the last step being done by a learned random-forest classifier[211] instead. An advantage of this technique is an increased versatility and generalizability to analysis of, e.g., non-contrast-enhanced images.

Demands on high-quality training data are tough with this approach, and with the limited amount of training data available, further mathematical processing of the training data using rotation invariant features[212,213], and a global optimization technique with graph cuts[214] was employed.

Specifically, the performance of the model[85] with regards to EATV was in-line with or slightly superior to earlier methods[215] (Dice-coefficient[216,217] of 0.91 for EATV), despite having the disadvantage of rather noisy images. A small negative bias[218] of < 2% was seen versus manual expert measurements. Processor usage and run times are both high with multi-atlas-based models, and were probably one of the reasons, why the research field migrated towards more efficient methods over the next couple of years, with more efficient use of computational resources[215,219]. In the meantime, it was clear that the availability of non-contrast-enhanced cardiac CT images by far outweighs the availability of contrast-enhanced images, not only in the SCAPIS-cohort, parts of which were at our disposal, but also in international research. Most published studies had also used non-contrast-enhanced images, probably for this very reason.

3.4 LESSONS LEARNED AND NEW CHALLENGES TO OVERCOME

It soon became evident that the task of properly measuring the EATV met with some tough challenges, the first of which was also the most obvious: human anatomy and its unpredictable variations, which would invariably cause problems in large datasets. The variations in the shape of the heart itself are relatively small, but the variations in the relation of the heart to surrounding tissues is immense, with also the need of taking the three-dimensional rotation of the heart with respiration into account. A reference dataset of much wider coverage of relevant anatomic variants would certainly be needed.

A second, somewhat more surprising challenge surfaced when manually proofreading the automated segmentations and the segmentation masks showing the distribution of voxels classified as EAT: there were voxels dispersed within the volume of interest, i.e., within the pericardium, not only in the expected areas immediately deep to the pericardium and along the coronary sulci, but also more centrally, corresponding to the ventricles and atria. For obvious anatomical reasons, there can be no EAT in the blood-filled cavities of the heart, and it stood clear, that noise was the culprit. The standard

approach to quantify the EAT depends on counting all voxels within the volume of interest which have the attenuation of adipose tissue (-30 to -190 HU). The relatively low radiation doses increase the standard deviation of the voxel attenuation values calculated in the image reconstruction process, and the probability that any voxel belonging to the tissues deep to the EAT would be wrongfully classified as EAT, increases correspondingly. Visually, in some images, significant amounts of spurious EAT were detectable, while in others very little to none. This obviously had to be dealt with in order to obtain a model, which would measure the EATV in a reliable way.

A third, potentially devastating problem was identified, when manually scouting through unselected examinations of the SCAPIS-pilot study: in quite a number of cases, the heart was not completely represented in the image stack, most frequently the superior (in up to 18% of examinations) or inferior (in up to 12% of examinations) parts. Typically, only a few slices would be missing, but in severe cases, up to an estimated 30% of the heart could be missing. Two options seemed reasonable, either to exclude incomplete images from analysis, or to devise a method to compensate for the loss of data from the missing parts of the heart. The first solution would require an automated screening method to find the incomplete image sets, since it would be too laborious to do the screening manually, and it would also lead to a substantial loss of data, affecting the power of detection of the study. The second solution would require, in addition to the automatic screening method, a method to predict the correct EATV based on the parts missing…

3.5 DEEP LEARNING AND CONVOLUTIONAL NEURAL NETWORKS FOR FULLLY AUTOMATED EAT ANALYSIS

During the second half of the last decade, an ever-increasing number of publications began to emerge, which had utilized various aspects of “deep learning”[220,221] (DL) to solve segmentation problems in the medical field. In short, DL is a special area of “machine learning”[222,223] (ML), which in turn is an area fitting under the wider umbrella term of “artificial intelligence” (AI). By definition, DL employs a neural network with at least three layers, where the layering attempts to mimic the functional architecture of the human brain. This provides some advantages in terms of plasticity, especially when compared to traditional ML, where the pre-processing steps are dependent on input from human experts. Convolutional neural networks[93] (CNN) in turn,

represent a special subcategory of neural networks, which typically perform well in classification and image interpretation tasks. They are highly scalable and autonomous in feature extraction tasks, which is the first step in the identification of objects or regions of interest in images, and previously was done to large extent by manual input or, in the case of multi-atlas-based techniques, required cumbersome pre-processing steps in the analyses. Another key advantage is the possibility to expand a model, not only by adding an additional layer into any CNN, but by combining different CNNs into a larger network. CNNs require large to very large sets of training data and the training steps can be demanding by means of computational power, but they are significantly faster in their image analysis once fully trained, enabling a much faster processing of large datasets.

3.6 SOLVING THE CHALLENGES

A model architecture combining two CNNs was chosen, where the task of pericardium segmentation and EAT analysis was assigned to one CNN ("EAT-Net"), while the task of predicting any missing EAT in cases of incomplete images was assigned to a second CNN ("Crop-Net"), which in turn would be the second in line in the steps generating the final output of EATV and EATA.

The segmentations used in the first paper could be used as templates to generate whole heart segmentations of the non-contrast-enhanced images from the same individuals after some minor adjustments compensating for the slight rotational differences due to changes in diaphragm position. These were then employed as a first training set, yielding sufficiently qualitative output which could be refed as new training data after manual corrections, either as whole heart volumes, or as partial volumes. The steps were repeated until the model was deemed to be sufficiently saturated with manually redacted training data. In addition, data augmentation[224], consisting of various mathematical processing steps, was performed to modulate the manually segmented or corrected images and increase the amounts of available training data. To reach a correct estimation of EATV, EAT-net would have to omit any voxels within the heart volume, which were incorrectly classified as EAT based on the attenuation thresholding. The most robust way to achieve this seemed to be a correction based on anatomical features, since any purely mathematical filtering applied equally to the whole image would carry the risk of introducing its own errors. A separate training dataset consisting of 30 complete examinations was created, where areas certainly without any EAT were manually segmented, i.e., the ventricles and atria, large parts of the internal

aspects of the myocardium, and the lumina of the great vessels, naturally with a reasonable margin of safety, to not encroach upon areas of true EAT. This would enable the model to exclude most, if not all the voxels incorrectly classified as EAT owing to noise-related issues.

Incomplete images posed challenges of an entirely different kind with regards to the generation of training data. A possibility, which seemed tempting, and was decided on, was to take large numbers of complete image sets (n=866), and artificially crop these at different levels, whereby we would obtain incomplete images, which could be fed as training data to the model, with data of de facto EATV in each case to match the training against. Based on the distribution and severity of cropping present in our material, the limit for training was set at maximally 40% of the heart missing, which gave some safety margins.

3.7 VALIDATION AND PERFORMANCE

Segmentation performance was in line with that of the multi-atlas-based model in paper I, with a Dice-coefficient of 0.90, when testing against manual expert segmentations in 25 cases. A slight negative bias was present, with the model underestimating EATV by < 2%[225].

To evaluate the broader performance of the model, 1,400 automatically segmented examinations were visually graded as acceptable or not acceptable. For a segmentation to be acceptable, it had to fulfil one of the following criteria: a) the segmentation is perfect, with no improvements to be made, b) the segmentation has some small errors, which are unlikely to influence the measured EATV and lies within the quality range of the 25 cases used to calculate the Dice-coefficient. For a segmentation to be deemed not acceptable, the following criteria had to be met: a) the segmentation has substantial errors, which will likely influence the measured EATV, and b) the segmentation is outside of the quality range of the 25 cases used to calculate the Dice-coefficient. Adhering to these criteria, most segmentations were of sufficient quality (99.4%) with only a minimal fraction of the segmentations deemed to be unsatisfactory (0.6%, corresponding to 8 cases of 1,400). Half of the failed cases showed anatomic variations of major importance: a large hiatal hernia, left-sided diaphragmatic paresis, post-surgical esophageal reconstruction, and breast implants. In terms of measured EATV, the failed segmentations were within two standard deviations of the mean EATV for the 1,400 cases and

would presumably be difficult to detect in a large material without a specific filtering tool.

The missing EATV in incomplete image sets could be predicted with a maximal error margin of around 6% when Crop-Net was tested in 55 cases, where manual whole heart segmentations not used in the training of Crop-Net were available, and various degrees of cropping, i.e., missing slices were simulated. Excellent linear correlation between predicted and true missing EATV was seen (R of around 0.955).

3.8 IMPROVING THE MODEL BEYOND PLAIN MEASUREMENTS

From the validation work on a broader, unselected material it became evident that possibly failed segmentations need to be identified in order to either be removed from the studied material or corrected manually and re-analyzed. In large cohorts, it is simply not feasible to rely on manual quality-checking, which requires all the images to be reviewed and a decision to be taken in every single case whether imperfections and errors sighted are severe enough to warrant correction. The requirement for an automated procedure, which forms an integrated part of the analytic model, was established. The manual reviewing of the 1,400 cases, and experiences gained in the training steps of the model pointed to some common traits among failed segmentations, among which the most conspicuous was a tendency to include parts of neighboring structures, nearly always in the form of tongues or spikes. After some theoretical considerations, according to which the shape of the heart requires a certain degree of sphericity, and some experimentation with image processing thresholds, a method was devised, which in effect detects and measures deviations from the normal shape of the heart. The cut-off in volume difference was chosen based on the findings in the 1,400 cases probed, in a way that no truly failed segmentation would be missed, and the number of false positives would still remain manageable[179]. When later applying the model to another cohort of more than 5,500 individuals, 166 analyses were singled out as potentially failed. Among these, less than 25% showed differences in EATV of more than 10% upon manual correction.

3.9 STATISTICAL ANALYSES

Generally, unless requirements for normal distribution were met on testing with the Kolmogorov-Smirnov method[226,227], or assumed, non-parametric statistical tests were used. A p-value of 0.05 was considered significant, unless specifically stated otherwise.

In papers I and II the Dice-coefficient, error estimates and other descriptive statistics referring to comparisons between EAT estimates by the model(s) and manual expert measurements were presented with their mean values, in Bland-Altman plots, and linear regression plots with the Pearson correlation calculated when adequate. In paper II a random forest classifier[211,228] was used to assess the relative importance of numerous co-variates to EATV and EATA and the explained variance in EATV and EATA.

In paper III the cohort was subdivided into groups according to the severity of disorders in glucose metabolism for most of the analyses performed. Descriptive data was presented with its median and interquartile ranges. Pairwise testing for differences between groups was performed with the Pearson Chi-square test[229] and the Kruskal-Wallis independent samples test[230] for categorical and continuous variables respectively. Correlations between changes in EATV and EATA over groups was performed with Kendall's Tau test[231]. Uni- and multivariable linear regression analyses (ANOVA) were performed to test for associations between EATV, EATA, various co-variates and insulin resistance and the various glucose groups.

In paper IV the cohort was divided by sex and, for the majority of analyses also by the presence of coronary artery calcifications (CACS > 0). Descriptive data were presented with their median and interquartile values. Uni- and multivariable logistic regression analyses were performed for variables showing significant differences between CACS groups with EATV as the dependent for the binary outcome of CACS = 0 or > 0, while linear regression was performed in the group with CACS > 0. Gradient boosting model[232] analysis was performed to quantify the relative importance of predictors for the binary outcome of CACS = 0 or > 0. A Receiver Operator Characteristic (ROC)[233–235] analysis was done for the same binary outcome with calculation of the area under the curve (AUC) for the variables included in the regression analyses. The Matthews correlation coefficient[236–240] was calculated for prediction of CACS > 0 based on continuous variables.

In paper V a similar approach was taken as in paper IV, with sex-stratified analyses and the data split according to the presence or absence of abnormal QRS-T angles. The same statistical analyses were performed, although with some slight differences in variables analyzed.

Statistical analyses in paper I were performed in MATLAB[241], in papers II-III largely in SPSS[242] and to some extent in R[243,244]. All statistical analyses in paper IV and V were performed in R, using either proprietary coding or existing packages.

3.10 ETHICAL CONSIDERATIONS

The studies were ethically approved by the Regional Ethical Review Board in Umeå (#2010-228-31M), the Regional Ethical Review Board in Göteborg (#560-13), and the Regional Ethical Review Board in Uppsala (#2021-04030). Procedures were carried out in accordance with the principles of the Helsinki Declaration (World Medical Association, 2008), among which the following are especially important for the research done within the framework of this thesis:

that the privacy and confidentiality of personal information of research subjects (section B.11) is protected, and the impact of the study on their physical, mental or social integrity (B.23) is minimized,

that the importance of the objective outweighs the inherent risks and burdens to the research subjects (B.21),

that the research subjects must be adequately informed about the aims, methods, benefits and risks etc. of the study, that they may withdraw their consent to participate at any time without reprisal (B.24), and that consent should be in writing.

The process of obtaining ethical permits for the underlying studies (SCAPIS and IGT-Microbiota), from which data has been used has been rigorous. Several of the investigations carry potential risks not only to the personal integrity of the study participants in a wider sense but also to their personal health, since exposure to x-ray irradiation is an integral part of the study protocols. Specifically, the CT-protocols were defined so, that radiation doses would be kept at a minimum, while still allowing for the gathering of necessary information. In addition, re-scanning of study participants due to suboptimal

image quality should be almost completely evaded, with exceptions only in very flagrant cases of image acquisition failures.

The five studies included in the thesis are all based on data collected in the SCAPIS and IGT-Microbiota studies, and no further data collection or contact with the study participants has taken place. All data has been handled in pseudonymized form. Only the chief researcher of the group had access to the code-key, by which it would have been possible to decipher the pseudonymization. The potential to identify any of the participants based on their data should be exceedingly low, especially given the large number of participants, and the random selection process from census data. However, the potential for identification based on CT images is not zero. Therefore, very strict handling of the data was applied, with local storage only of unencrypted images, encryption of images prior to any transferring between co-workers during the development of the model, and limited use of images in both published and unpublished reports.

In any study recruiting previously healthy individuals, the finding of signs of undiagnosed disease could be challenging. In the design of the underlying studies, much attention was focused on the proper management of any unexpected findings suggestive of disease in accordance with best medical practice.

4 RESULTS AND THEIR DISCUSSION

4.1 PAPER I

Two experts prepared the ground truth segmentations of the pericardium in 30 whole-heart contrast enhanced CT image sets independently of one another. The inter-reader agreement was excellent, with a Pearson correlation coefficient of > 0.99 and a Bland-Altman bias of -4.7% (mean EATV of 103.34 vs. 108.44 ml). The Dice-coefficient, which is a reliable measure of the geometric overlap of two structures, in this case segmentations, was 0.90 between the two expert readers when looking at total EATV, while it was 0.98 when looking at the total volume within the pericardium. The discrepancy between the two Dice-coefficients is simply explained by the fact, that all the variation between the two readers will be found peripherally, while almost all the EAT is also located peripherally in the segmented volume. Naturally, the relative impact of variations in segmentation on the much smaller EATV will be greater than for the total intrapericardial volume. The relation between the numbers gives an idea of the needed precision in segmentations of the pericardium, also hinting to its theoretical upper limit, since even minute differences geometrically in how the pericardium is traced by the experts will translate to significant differences in EATV.

The multi-atlas-based model developed showed an agreement with the manual expert measurements (expert 1) which was superior to the agreement between the two experts. A Dice-coefficient of 0.91 and 0.97 for EATV and total intrapericardial volume respectively was calculated. This by itself places the performance among the very best reported in the literature, and with respect to the inter-reader agreement, seems to be near the upper theoretical limit of what is feasible to reach. A minuscule Bland-Altman bias of +0.78 ml was found between the EATV of the model and expert segmentations. The mean EATV measured by the model was 109 ml, which is reasonably close to later measurements in paper II, and also harmonizes well with reported values in the literature. Of course, the small number of individuals included in this study limits the scope of conclusions that can be drawn, especially with regards to the validity of the results in images from a broad, unselected population, where anatomical variation could interfere with performance.

4.2 PAPER II

The manual whole-heart segmentations (29 out of 30) used in the first study were successfully co-registered with the corresponding non-contrast-enhanced CT images, requiring only minimal manual intervention to create an initial training dataset. Incrementally, the model was refed with manually reviewed and/or corrected segmentations ranging from single slices to whole heart volumes, until saturation was reached with a training set of 308 individual CT examinations in total.

A mean Dice-coefficient of 0.90 for EATV was reached when testing against ground truth, which consisted of a new set of 25 manual expert segmentations of the pericardium in the whole heart volume not previously used in the training steps, all prepared by one expert. Mean EATV was 106.7 ml with a small negative Bland-Altman bias (-1.76 ml, or about -1.6%) present. The relative error in the automated EATV measurements was less than 12% in all cases, with a mean of 4.7%. The technical performance with respect to segmentation precision was in other words almost identical to the results obtained in the first paper, despite the fact, that the models are fundamentally different in their segmentation approach, and non-contrast images were used instead of contrast-enhanced images.

Noise-induced effects on the thresholding-based classification of voxels as EAT or non-EAT were obvious on visual examination, ranging from stray voxels within the heart chambers to rather significant confluences of areas incorrectly marked as EAT. After training the model on recognition of the heart chambers and parts of the myocardium, these noise induced effects on the classification of EAT were, if not eliminated entirely, reduced significantly, with a more than 11% improvement in the relative error of the EATV estimation (from 5.31% to 4.7%).

Unfortunately, many of the CT examinations in the SCAPIS material are incompletely representing the heart, with parts of usually the most superior or inferior parts missing. To remove these would require substantial manual work, and at least reduce the number of examinations available, if we assume that the problem is randomly distributed among study participants. Our approach of training a second CNN-based model to predict the correct EATV in afflicted cases proved to be useful – correct predictions could be made within an error margin of 6% for examinations, where up to 40% of the heart

was missing. In the most relevant range with up to 10% of the heart missing, a relative error of less than 1% was achieved.

As part of a broader validation, a thorough visual examination of each slice in 1,400 CT examinations was performed, and 99.4% of the whole heart segmentations were found to be of acceptable quality, or in line with the performance metrics accounted for in the 25 benchmark cases. A mere 0.6% of the reviewed cases represented failed segmentations, where significant errors were present, deemed to probably influence the measured EATV. Curiously, all of them had an EATV within two standard deviations of the mean EATV in the 1,400 cases, which was 113 ml (range: 22-320 ml). Our EATV lies in the mid-tier of reported values in the literature, however, there is considerable variation among previous reports, accounted for by the many various methods, from manual, over semi-automated to fully automated, in some cases even with varying thresholds for EAT classification.

Substantial co-variation was seen with anthropometrics for EATV in a gradient boosted model analysis using random forest classifiers. Waist circumference and weight was found to have the highest importance, accounting for over 40 and 30% respectively of the increase in mean squared error, while the entire statistical model could explain just above 40% of the variance in EATV.

EATA was found to be strongly correlated to EATV, with the latter accounting for around 75% of the increase in total mean squared error in the statistical model, explaining over 55% of the variance. If we assume that an expansion in EATV is mainly mediated by an accumulation of lipid content in the adipocytes of the EAT, the findings of lower EATA is entirely logical, reflecting the lower radiodensity of lipids compared to the other components of the EAT.

4.3 PAPER III

The model developed in paper II was used on images from 1,948 individuals from the IGT-microbiota study, representing a population sample enriched for individuals with various degrees of glucose disorders. The same image-acquisition parameters as for the SCAPIS images used for the training of the model had been used, which obviated the need for re-training of the model. An automatic quality checking algorithm of the segmentations was tested and validated in 400 of the examinations, which were manually reviewed to test the reliability and find a reasonable cut-off. In the entire cohort comprising

1,948 CT examinations 28 were singled out as potentially failed by the model, out of which 13 cases of true failures were identified (or about 0.7%) requiring manual corrections. The types of segmentation errors encountered in failed cases reflected the findings among the 1,400 cases in paper II.

The cohort was subdivided according to classes of glucose disorder into normal glucose tolerance (NGT), impaired fasting glucose (IFG), impaired glucose tolerance (IGT), combined glucose intolerance (CGI) and type-2 diabetes (T2D) with stratified analyses across the groups. The median EATV was clearly increased in the T2D group compared to the NGT group (146.6 vs. 104.9 ml). EATA showed a strong negative linear correlation to EATV in the entire cohort, with lower values seen with increased EATV. The differences in EATA over the glucose groups were however small (-72 HU and -69 HU respectively in the T2D and NGT groups). EATV was highly correlated (R=0.739) to abdominal visceral adipose tissue area (VATA) in the NGT group, measured according to the method described by Kullberg et al.[245] as the adipose tissue quantity in a CT slice over the mid-abdomen. VATA is considered a reliable measure of abdominal obesity and was included in a stepwise multivariable logistic regression analysis over the glucose groups together with other co-variates and confounders such as age, sex, smoking and anthropometrics. It was clear that no independent effect of EATV or EATA remained after introduction of VATA into the statistical model, and that the co-variation with the other variables was marked.

The results obtained confirm findings in previous reports that there is indeed a tendency to increased EATV with increasing derangement of the glucose metabolism, while there seems to be a reduction of EATA at least in T2D compared to NGT. Most studies are relatively small, and very few studies have reported on pre-diabetes. In pre-diabetes, contrary to what was seen for EATV, the reduction in EATA was independent of BMI and waist-circumference, but not VATA. This might suggest that EATA could be a more sensitive parameter than EATV for early pathological changes in glucose homeostasis. Although there is reasonable doubt to the precision in EATA estimates, the relevance of the findings should neither be overstated nor understated, especially not since global EATA measurements in this case reflect the effects of a systemic metabolic disease.

4.4 PAPER IV

The cohort investigated in paper III was further explored with focus on the presence of coronary artery calcifications, or a CACS > 0. Valid CACS data were available for 1,945 individuals. Since the cohort was enriched for pre-diabetes and T2D, statistical analyses were, when applicable, proportionally weighted to compensate for effects on single variables in regression analysis.

We were not able to find any association between EATV, EATA or CACS > 0 in any of the statistical analyses, when adjusting for anthropometrics and co-variates. Age and sex were the most significant co-variates, with the largest relative importance. These results support the trend in the literature, where a significant and independent association has been found in several studies between increased EATV, as well as locally decreased EATA around the coronary arteries, and major adverse cardiovascular events, while no convincing evidence is available to support an independent association between EATV and coronary artery calcifications, when adjusting for relevant co-variates. For detailed results, the reader is referred to the manuscript due to potential copyright issues upon future publishing.

4.5 PAPER V

A sub-cohort of the SCAPIS including 5,571 individuals with valid CT and VCG-data was investigated with regards to a possible association between QRS-T angle abnormalities and EATV or EATA. Individuals with known previous heart disease, e.g., myocardial infarction, were excluded to reduce any confounding effects by previous myocardial damage. No differences in final statistical results were seen, when these patients were later included in the analyses as a sensitivity test.

EATV and EATA was automatically analyzed with the final model used in papers III and IV, and the automatic quality checking step flagged a total of 166 whole-heart segmentations as potentially failed. Every one of these was manually reviewed and, if needed corrected in its entirety, then re-analyzed. Less than 25% of the segmentations showed more than 10% difference in EATV after manual correction, which corresponds to about 0.7% of all the automatic analyses (5,571). Surprisingly small differences were seen overall, with a median difference in corrected versus uncorrected EATV of around 5%.

There were considerable disparities between men and women with regards to the presence of abnormal QRS-T angles, and all analyses were performed separately in the two groups. Despite this, no significant association was detected between abnormal QRS-T angles and EATV or EATA. The reader is again kindly referred to the manuscript for a detailed description of the results.

5 GENERAL DISCUSSION

5.1 THE MODEL AND ITS PERFORMANCE

There is a trend towards fully automated segmentations in this area of research, which has been cemented lately, with several technically successful models, among which the one presented by Commandeur et al.[95,122,123,141] stands out in that it has been tested in larger cohorts. There is much to be commended, but there are also shortcomings, most prominently a deliberate omission of the most inferior part of the heart volume, which introduces an uncertainty to the validity of their results. It can be argued that only a minor part of the EAT is excluded, but it is not known how large this part is, and if it de facto varies between individuals based on anatomical configuration of the heart. Recently, West et al.[99] proposed a technically fairly similar model, which was tested in both 3,720 cases from the ORFAN cohort, 1,558 cases from the SCOT-HEART cohort and a third, smaller cohort of 253 cases post cardiac surgery. From a technical point of view, it seemed to perform well, although the Lin Concordance Correlation Coefficient[245] was used instead of the more established Dice-coefficient for evaluation of segmentation accuracy, which makes a direct comparison between the models difficult. The preparation of ground truth, as well as the anatomical limits of segmentation are not described in detail, but it seems from images of automatic segmentations, that an approach similar to the one used by Commandeur et al. might have been chosen, omitting the most inferior parts of the heart. The median EATV reported by West et al. is higher than in most studies and shows substantial differences between the tested cohorts (ranging from 121 to 169 ml) despite similar BMI, which raises some questions about the robustness of the model. In our largest cohort, we obtained a median EATV of 108 ml from 5,571 automatic analyses, from which 37 were manually corrected after being reviewed among the segmentations singled out by the model's quality checking feature. This estimate of mean EATV is closer to the weighted average of 99 ml reported in a selection of important studies, mainly based on semi-automatic analyses[225]. There is generally very limited to no information on the failure rate of published automatic models, which clouds the assessment of their applicability in an unsupervised manner in large cohorts, where anatomic variation is expected.

A problem which we encountered and recognized early in our work, was the problem of noise-related misclassification of voxels on thresholding and

calculation of the EATV. This issue has not been sufficiently, if at all, addressed in publications purporting to have solved the task of automatic measurements of EATV and EATA. We find it difficult to believe, that noise-related artifacts would be exclusive to our material, even though we have higher noise levels than many studies due to our strict protocols for limiting radiation exposure. In our material, when estimating the effects on the relative error in EATV calculation, noise suppression improved the accuracy to an extent which is hardly negligible. The more than 11% average improvement in relative error (translating to an improvement of about 0.5% in estimated EATV) might be equally distributed in a material, but if not, could affect results significantly in cases severely affected. Upon visual evaluation of 1,400 examinations, we found that widely varying effects of noise were present, without any clear tendency to be more common in individuals with large hearts or much adipose tissue either subcutaneously or intrathoracically. Instead, the impression is, that the effects of noise are randomly distributed, which makes the problem more unpredictable in terms of potential effects on results.

Incomplete image sets, with parts of the heart missing, could introduce grave errors in automatic analyses, unless detected either by manual screening, corrected or removed manually, or corrected automatically in an integrated step of the EATV estimation. There is little to find in the literature on the problem of incompletely imaged organs with relevance to this research field. However, it is plausible that other research groups would also have had to deal with the problem, where parts of the heart are missing due to misplaced scanning volumes or patient movement. In our material, cropping, or omission of the most peripheral parts of the heart volume, was seen most frequently superiorly and inferiorly, with less than 10% of the slices missing, but extreme cases coming close to around 30% of slices missing. The CNN-based model for prediction of the correct EATV in incomplete cases showed a mean relative error in EATV of less than 1% if up to 10% of slices were missing, and in the most extreme cases a mean relative error of just slightly above 5%.

Automatically identifying failed segmentations, which seems to be a unique feature of our model, is very important when applying the model to large datasets, since manual proofreading can be exceedingly time-consuming. The true failure rate of the overall model in segmenting the pericardium has been constantly around 0.6-0.7% of segmented cases, when tested first in 1,400, then in 1,948 and 5,571 CT examinations. All failed segmentations were correctly flagged by the automatic quality checking step, while the total number of flagged cases were kept at a manageable level of around 3-4% of

cases, i.e., in a series of 30,000 cases, around 1,000-1,200 would have to be manually reviewed, and out of these, about 200 would have to be manually corrected in some way to be of acceptable quality.

In summary, the model developed by our group shows a technical performance, measured as the Dice-coefficient, or geometric overlap between automatic and manual expert segmentations, in line with or superior to competing models, while it also presents a practical solution to the suppression of noise-induced misclassification of EAT, a highly accurate prediction of correct EATV in cases of incomplete, or cropped images and a very sensitive and reasonably specific quality checking step, which ensures that no failed segmentations/analyses are let through. Repeated manual reviewing has confirmed the robustness and capabilities of these built-in extra functions, which greatly enhance the model's versatility.

Doubts as to whether fully automated measurements of EATV are reliable are always relevant but have not been extensively discussed in the literature. Manual segmentation of the pericardial contour has long been regarded as the reference method, with all its drawbacks, not only in terms of high workload and inter-reader discrepancies, but also the variance in intra-reader precision, especially in large series of analyses. We know from the literature that an inter-reader agreement corresponding to a Dice-coefficient of around 0.9 can be expected at best[86,246–248], which was also confirmed in our own work (in paper I). The reason for not reaching higher is likely to be found in the inherently complex task of delineating the pericardium properly, since it is not always visible in every slice, meandering through adipose tissue and at times bordering soft tissues with very similar radiodensity. One definite advantage of an automated segmentation method should be its uniformity in performing the given task, with a predictable error rate, which is independent of any changes in outer circumstances. During the manual reviewing process in the validation of the model, an intriguing, and somewhat surprising finding was, that the model´s segmentation performance was not systematically visibly worse in cases of exceedingly noisy images, where manual segmentation would have met with greater problems. The robustness of the model, which uses various features by which to identify the pericardium correctly, and the training of which has included large quantities of images as well as their augmented derivatives, seems to surpass that of a manual expert, at least when it comes to purely image technical parameters. Naturally, when it comes to anatomical variations and their recognition, beyond what is to be expected from the training material used in the development of the model, a less

impressive performance is to be expected. The effects of this were also seen in the identification of the failed segmentations, when the majority of these represented rare or unexpected anatomical variants. Altogether, we believe it is correct to state that the model presented is a superior alternative to manual measurements and has remedied the shortcomings of previously published automatic models for EAT analysis.

5.2 POSSIBLE SHORTCOMINGS AND PITFALLS

Automated image analysis, irrespective of the precise technical parameters of the model used, is always dependent on the quality of the data with which the model is fed and trained[92,94,249,250]. The adage "rubbish in – rubbish out" couldn't be more correct with regards to the problems facing all developers or researchers in the field. One fundamental question is whether to use manual training data from as many experts as possible, or on the contrary, as few as possible. The former solution carries the advantage of averaging out possible systematic errors made by individuals, while the second has the advantage of presenting a more homogenous set of training data with less of idiosyncratic variation due to individual interpretation of anatomical landmarks and their like. In our case, training data has been produced solely by one expert. In the extreme case, this could be a catastrophic mistake, in the other extreme a blessing, since training data can be assumed to be highly consistent, which is undoubtedly a prerequisite for successful training of any model.

Segmenting the pericardium involves more of educated guessing, than many other segmentation tasks in medical image analysis, where anatomical boundaries are less obscure[1]. As we could see in our own inter-reader analysis of 30 whole-heart pericardial segmentations, which were performed in the three orthogonal planes, there were not only differences quantifiable as the geometrical overlap expressed in the Dice-coefficient, but also a systematic bias, expressed in the Bland-Altman function. The latter could and should be interpreted as a result of the reader-specific differences in the educated guessing as to where the pericardium is located, when not fully or clearly visible[85]. Instructions as to how to draw or segment the pericardial contour were very specific and could hardly have left room for any personal interpretation. Moreover, since the pericardium is exceedingly thin over most of its course, the placement of the Bézier curve should have been quite self-explanatory when the location of the pericardium was certain.

We believe that our choice of limiting the preparation of training data to one expert has reduced ambiguity in the training steps and might have contributed to the excellent results with regards to the accuracy and versatility of the model. At this point, one could object, that testing was also done against manual segmentations performed by the same expert. That might be a relevant issue, but if we accept that no expert is "better" than any other at finding the true course of the pericardium, this is of less importance if overall performance of the model is improved. The thorough and systematic visual examination of segmentations in paper II should compensate amply for any potential doubt regarding the practical usefulness, since the 1,400 cases included provide a broad anatomical variation. Also, a third expert, not previously participating in the segmentations visually examined the quality of the segmentations performed by the expert preparing the testing data, to make sure that the identification of the pericardial contour was anatomically correct.

The fact that the testing samples were small in both paper I and paper II, consisting of only 25 whole-heart segmentations in the latter, could be held against our claims and our results. A larger number of manual segmentations to test against could have yielded different results, but we believe that the anatomical variation among the 25 cases represents an adequate level, and that a substantial increase in the number, say to 50 or 100 cases, would have carried a disproportionate extra workload, with a possible narrowing of the confidence intervals of the Dice-coefficient and the error estimates. The fact that the visual evaluation of the 1,400 automated segmentations showed, that only 0.6% of them were of worse quality than the test cases, speaks against any large effects on the calculated performance metrics by a hypothetical increase in the number of test cases. The manual corrections of 166 cases of potentially failed segmentations by the model in paper V also gives credit to the accuracy data presented in paper II. Both the frequency of true failures (0.7%) and the relative error in the estimated EATV of the model (median of around 5%) versus the manually expert segmented EATV were comparable.

5.3 METHODOLOGICAL IMPORTANCE OF OUR RESEARCH

Exact and correct measurements of EATV and EATA are a prerequisite to further explore possible associations with known risk factors or the disease processes themselves. A high level of accuracy can be obtained by manual segmentations and the supervised thresholding and subsequent calculation of

EATV and EATA from CT images. The workload is however extensive, and the accuracy reader specific, making direct comparisons between different studies with various readers harder than for automated methods. Numerous models have aimed at an accuracy similar to that of manual measurements while reducing the time for analysis[77,215,251]. The semi-automatic models have partly solved the problem, but reader-specific accuracy remains an issue. The automatic models proposed have, to varying degrees, reached at least an accuracy comparable to manual measurements but left other questions unanswered[83,86,95,96]. Multiple challenges have been identified over the course of development of our own model, to which we have proposed specific solutions: the problem of incompletely imaged hearts, the problem of noise-induced effects on EAT-classification, and the problem of identifying the unavoidable failed segmentations produced at a low, but certain rate. All in all, the model represents an analytical tool with extended capabilities, which should be well suited for the investigation of EAT in large scale population studies. It is not yet proven that the model can be adapted to any kind of CT images, but its development history and design suggests, that this might be the case at a fairly low cost. If proven to be adaptable, the model, or any further developed version of it could be used in a wider community, enabling direct comparison on the same conditions between data from different studies. However, this needs to be specifically investigated, preferably in a multi-center study, where the model could be compared not only to other models, but also to manual expert measurements on images obtained from CT machines from various vendors, which typically have differences in their proprietary image reconstruction algorithms[252–254], resulting in, at least visually, varying image characteristics.

5.4 EATV AND EATA DATA IN THE LITERATURE

Numerous studies have reported EATV from CT images over the years, but striking discrepancies are seen upon a closer look, even though the investigated cohorts have reasonably similar anthropometric characteristics. There are of course considerable methodological differences between studies representing work done over the past fifteen years. Initially only manual segmentation of the pericardium was available, then various semi-automatic methods were used, until lately, when some fully automated analytical software solutions have emerged. The main issue with manual methods is their cost of labor, which in large studies actualizes the need for multiple persons performing the

segmentations. Both inter- and intra-reader variability increases the uncertainty of the results, although it could be argued, that these are mitigated if large enough numbers of images are analyzed.

Significant differences exist in the literature with respect to the parts of the heart, which are included in EAT analyses, in the most extreme being limited around the coronary arteries[255,256], in others limited to partial volumes[257,258] or almost complete volumes[99,141,259]. Even among methods which strive to measure the entire EATV, the variation in obtained results is considerable, with the results reported in methodologically important works ranging from 86[73] to 159 ml[142] in median or mean EATV. In the latter work Marwan et al. investigated the effects of contrast enhancement, the x-ray tube voltage used, as well as various thresholds for EAT classification, and could verify that all parameters significantly influenced EATV estimates. To successfully sort out the causes for EATV discrepancies in various studies, it should be kept in mind, that the tube voltage used in some instances is less than the usual 120 kV, which seems to have become the unofficial standard[260], and also, that the thresholding limits for EAT classification vary somewhat across studies. In the case of Mahabadi et al.[73], part of the explanation to why their median value is as low as 86 ml might be revealed by the fact that they used a narrower interval of -45 to -195 HU, which could, if the results of Marwan et al.[142] are to be trusted as generalizable, account for a difference of somewhere between 18 and 34 ml, compared to if they had used -30 HU as the cut-off. In other words, even when trying to compensate for differences in technical parameters, the picture remains unclear, as to where the truth lies. In a small, but strikingly original work, Hindsø et al.[261] investigated the EATV post-mortem in eviscerated hearts with CT and found mean values corresponding to 65-73 ml for women and men respectively. They used the standard 120 kV tube voltage, and it can be argued that there was very little room for misclassification of tissues in their case, given that the pericardium had been properly anatomically dissected. What makes the use of their values difficult as a reference is the fact, that the organs had been drained for blood and that some of the volume of the EAT could have been lost in this process as well as due to other changes post-mortem. However, their study sets a kind of lower limit to what can be expected when running the analyses in vivo, if the EAT is properly segmented and separated from the surrounding, paracardial adipose tissues.

Estimation of the EATA is even more sensitive to the various influencing factors. Tube voltage affects noise levels to begin with, with lower voltages showing more noise, and consequently more noise-induced misclassification

of voxels as EAT would be expected. Secondly, HU-levels of any given voxel are directly proportional to the tube voltage[48,262–264], making unadjusted comparisons over different studies difficult, unless the same voltage has been used throughout. In some methodologically important works accounting for the EATA at whole-heart level, reported mean or median values cover a range from -73.4[24] to -80.8[23] HU, the former being the mean in individuals with no signs of metabolic syndrome, the latter being the median in individuals with T2D. In the first study Lin et al. showed an absolute difference of only 3.5 HU (-73.4 vs. -76.9 HU) between the groups compared, while at the same time the difference in EATV was 40.4 ml (73.7 vs. 114.1 ml). The second study by Milanese et al. had an even smaller absolute difference in EATA of only 2.6 HU (-78.19 vs. -80.78 HU), while EATV differed 30.3 ml (82.62 vs. 112.87 ml). It is obvious, when reviewing these numbers, that the interval which the mean or median EATA measured at whole-heart level is spanning, is narrower than for EATV. This might reduce the validity of results, generally speaking, since even minute errors in the estimation of EATA could have profound effects on the small differences. However, the findings in various cohorts seem to be remarkably coherent, when pointing to a trend of decreasing EATA in the setting of either pre-diabetes or T2D, or coronary artery disease, conditions which are both associated with increases in EATV. When zooming in on the smaller volumes of EAT immediately in contact with or surrounding diseased segments of the coronary arteries, the absolute differences of peri-coronary attenuation values reported are small, 1.1 HU in a study by Goeller et al. comprising 293 individuals with varying degrees of coronary artery disease[265]. In a study on 134 patients receiving biological anti-inflammatory therapy, peri-coronary EATA was found to decrease more conspicuously, from -71 to -76 HU[266]. Even larger absolute differences in peri-coronary EATA were found in a study by Kwiecinski et al.[267] around high-risk plaques on CT which also demonstrated ^{18}F-NaF uptake on PET, having median values of -73 HU versus -86 HU for plaques without these features. In effect, these reports point to greater pathophysiological relevance of the EATA at a local level, with measured differences likely increasing with the specificity of the findings.

5.5 EATV AND EATA DATA IN A PHYSIOLOGICAL AND PATHOPHYSIOLOGICAL CONTEXT

Changes in EAT can be both physiological and a sign of pathological processes taking place, in some instances a harbinger of later adverse events. Although

longitudinal studies on the natural history of EAT, and therefore the physiological changes over time, are scarce, there is some evidence suggesting that EATV increases with age[9]. Conversely, EATA, which is strongly inversely correlated to EATV, is expected to decrease with age. The latter process is likely further augmented by the fact that the relative amount of brown adipose tissue generally decreases with age[19], although there is substantial variation. Some seasonal variability in brown adipose tissue activity, and consequently EATA has been shown[18], but this seems more relevant in a younger age group than the target of most studies involving EATV and EATA. We could not, for instance find any statistically significant differences in EATA between individuals examined during the winter season compared to the summer in paper III. Age shows a co-linearity with EATV in most studies where age is included as a variable, but the amount of contribution from normal ageing is not easily clarified, since most disease processes also advance with age. The question of sex and its importance in the investigation of EAT is both highly relevant and more multi-faceted, than what is apparent at first. The obvious differences in body size, present also in the internal organs, including the heart, has a direct effect on the measured EATV, where men with no known heart disease in our largest cohort studied had clearly higher EATV (124.1 vs. 94.4 ml). Unsurprisingly, EATA was correspondingly lower in men (-70 vs. -69 HU). However, regardless of the purely anthropometric differences, there are differences possibly mediated by sex hormones. It is a well-known fact that men are prone to cardiovascular disease development at an earlier age, whereas women seem to be protected until menopause[268,269]. There are few studies reliably accounting for menopausal status among women, something which could complicate the interpretation of data, unless the age span of the cohort clearly makes this detail irrelevant.

No large-scale studies with more than five to ten thousand participants have investigated the EAT in relation to coronary atherosclerosis, while there are some in the interval of one to five thousand participants[73,75,99,122,125,144,270,271], and plenty of smaller studies. Noteworthy methodological differences often make direct comparison difficult, but from some systematic reviews, it seems to be beyond doubt that an increase in EATV is associated with an increased risk of various cardiovascular adverse events, even when adjusting for age and other relevant co-variates[14,15]. The picture is more ambiguous, when it comes to linking EAT to coronary artery calcifications, with most studies, including our own finding little support for any independent association. So, why is this discrepancy interesting at all? If we look at how the EAT was first "discovered" as a potential area of interest in research oriented towards

cardiovascular disease, we find that an increased inflammatory response was demonstrated in the EAT[6]. At a local level, immediately next to the coronary vessels, it seems logical to assume, that the supporting tissues, i.e., the EAT, would participate in any pathophysiological processes evolving. Imaging techniques available in vivo, with the possible exception of intravascular ultrasound (IVUS)[107] and optical coherence tomography, have a resolution limit, which unfortunately doesn´t really allow any selective gathering of truly local information. Although formidable technical advances have been achieved in the field of CT[272], the resolution remains practically at 0.3-0.5 mm, limited by hardware-specific noise[60,204] and unavoidable artifacts introduced in the process of image reconstruction[252]. Changes in the attenuation of the EAT in the vicinity of the coronary arteries, the periarterial or pericoronary EAT, have been extensively investigated[21,22,35,150,203,265–267,273–278], and some promising results with regards to a possible connection with the pathophysiological processes governing the build-up of atherosclerotic plaques have been shown[279,280], although some questions remain in relation to the influence of anatomy[281], sex[282], contrast administration[46], as well as changes in the pericoronary EATV[283]. In light of these findings, one would instinctively have wanted to demonstrate an association, independent of general anthropometric or laboratory-based risk factors, between the appearance of calcifications in the vessel walls and changes in the EATV. Coronary artery calcifications represent not only an important sign of atherosclerotic involvement[284,285], but also a very easily detectable one on CT, with few potential confounding factors present anatomically in the volume of interest. This might be the reason why coronary artery calcium scoring, as described by Agatston et al.[45], has been so universally adopted in clinical use. Due to the distinct difference in attenuation, calcified tissue is easily spotted as well as segmented, be it manually, semi-automatically, or fully automatically[286–288]. One would perhaps incline towards the assumption that the absence of calcifications, or a CACS of zero, would mean that the individual is free from atherosclerotic disease. However, as shown previously, this is not necessarily the case[111,117], and the processes governing calcification seem to be more complex than being directly related to the appearance of atherosclerotic plaques[289–292]. If we assume that the pooling of relevant studies performed in the systematic reviews[14,15] addressing the relationship between EAT and atherosclerosis is correct, and the underlying studies are indeed credible, we may conclude that EATV, and EATA, at least locally, are probably more specific markers of early atherosclerosis than the CACS, and some classical cardiovascular risk factors. A possible clue to why this might be the case is revealed in the studies of EAT in pre-diabetes and T2D. It is well established, that the EATV expands as the glucose metabolism

is increasingly impaired[17,171–176,255]. We could confirm these findings in our work (paper III), but the changes were not independent of VATA. Diabetes is one of the prime risk factors for the development of atherosclerosis[293–296], both at micro- and macro-level, and the changes are often preceded by metabolic changes by years, if not decades. Consequently, it is not too ostentatious to raise the question whether the EAT, might not just very well be a good gauge of early metabolic changes, which influence the course of coronary atherosclerosis. In early pre-diabetes, our findings of a generally lower EATA potentially points to a difference in dynamics in the processes responsible for the EAT expansion seen in diabetes. An early accumulation of lipids, later followed by inflammatory and fibrotic changes in the EAT, which could influence the atherosclerotic processes, would be a tempting hypothesis to test in a larger, preferably prospective study. At the same time, coronary calcifications detectable by CT might be late symptoms of atherosclerotic disease, or more like the evidence found at a crime scene, but not the perpetrator or motive itself, which somewhat limits the prospects of finding reliable answers with only radiological methods. It should at this point be stressed, that, although our model is not at present capable of differential measurements over anatomical territories and local effects on EATV or EATA are likely to be overlooked, any further development allowing for local measurements would probably still have insufficient spatial resolution to elucidate the precise mechanisms of the proven discrepancies between CAC and EAT findings.

Likewise, when investigating the possible association between EATV, EATA and abnormal QRS-T angles on vector electrocardiography, we were not able to discern any statistically significant relationship. Ernault et al. has comprehensively reviewed the literature on the possible pathophysiological importance of the EAT for the development of arrhythmias[297] and the strongest case in the literature seems to be a connection to atrial fibrillation. In a meta-analysis by Wong et al. EATV was found to exhibit stronger association to atrial fibrillation than general or abdominal adiposity[298], and in a small, but methodologically robust study, Al Chekakie et al. found that EATV was associated with atrial fibrillation among 273 individuals after adjustment for traditional risk factors including age, sex, BMI, hypertension and diabetes[299]. The causes remain less clear[200,297,300] and largely hypothetical, while even less is known about the potential effects of the EAT on the electrophysiological processes in the ventricles. Among the suggested causative mechanisms[301–303], fatty tissue infiltration into the myocardium as well as secretion of inflammatory substances could provide clues to the observations, that

abnormal QRS-T angles seem to be a marker of the risk for sudden cardiac death[193,194]. If we accept the proposed connections between the EAT and arrhythmogenesis as plausible, it is necessary to raise the question why an association between EATV and atrial fibrillation is so well documented, while the association between EATV and ventricular arrhythmias is so scarcely documented. A possible explanation lies in the much larger mass and volume of the left ventricle, as compared to the atria, which would absorb much larger amounts of endocrine or mechanical influence from the surrounding EAT than the atria. In our material, although representing a very large cohort in relation to previous works on QRS-T angle abnormities and EAT, the participants were free from known cardiac disease and represented an age group of 50-64 years, where at least for the female participants, a relatively low prevalence of atherosclerotic changes would be expected. Of course, the absence of a demonstrable connection between EATV and EATA at whole-heart level, as measured by our model, doesn't exclude the possibility of local effects mediated by processes in the border-zone between the EAT and the myocardium, which are immediately contiguous.

6 CONCLUSIONS

A model capable of fully automated analysis of EATV and EATA in CT images has been developed and tested in two cohorts, together comprising more than 7,500 individuals. An accuracy in EATV estimation equal to manual expert measurements is possible for both contrast enhanced and non-contrast enhanced CT images, and can be expected in large series of analyses, with a segmentation failure rate of consistently around 0.6-0.7%. Any failed segmentations can be found automatically by a built-in quality assessment step.

Noise-related effects on the attenuation values of the smallest image elements, the individual voxels, can be considerable and influence their classification as EAT or non-EAT. The effects of noise are expected to be more prominent in images acquired with low radiation doses but seem to be randomly distributed with regards to anthropometric data. Anatomically based noise-suppression, which is an integrated feature of the developed model, significantly reduces the error in EATV estimates due to wrongly classified EAT.

In all large series of cases, incompletely imaged organs are to be expected at some rate. The model has been trained to recognize if any part of the heart is missing, and in these cases to predict the correct EATV with very high accuracy. This feature reduces the need to manually quality-check images used in a study and reduces the need to discard data.

From our experimental data it is clear, that EATV varies in a relatively wide range in the population in the age-span of 50-64 years, with men having significantly higher EATV compared to women. In a population enriched for pre-diabetes and T2D, EATV is significantly increased in the groups of advanced pre-diabetes and T2D, while EATA is significantly reduced. A strong inverse correlation exists between EATV and EATA, where lower EATA is seen in individuals with high EATV. There is substantial co-variation of EATV and EATA with VATA, age, anthropometric data, and many laboratory parameters, findings which generally correlate well with previously reported data in the literature.

In specific analyses of EAT and its possible association with coronary artery calcifications or QRS-T angle abnormalities in images from the two cohorts at our disposal, no independent association could be verified. These findings don’t exclude potential links at a local level, adjacent to the coronary arteries or the myocardium, since the model only accounts for EATV and EATA at

whole-heart level. Also, the findings might be valid only in the examined age group, with potentially different outcomes in a much older population, where the prevalence of coronary atherosclerosis would be higher and sex-differences in both EAT characteristics and disease burden can be expected to be less pronounced.

7 FUTURE PERSPECTIVES

The model will be used more widely in research within the framework of the SCAPIS study. CT images from the entire cohort of around 30,000 individuals are ultimately set to be analyzed with regards to EAT data. Among possible further feature developments for the model, a capability to identify the periarterial EAT and to gather data on it specifically, is high on the wish-list. Results and material from parallel research focused on the coronary arteries and their morphology could be used for training or integrated into the model, unless a de novo approach is chosen.

Irrespective of any further addition of features, if the model can be successfully adapted to other cohorts with different image characteristics, possibly after some re-training, its versatility will be increased, allowing it to be used in a wider scientific community and, if applied in large enough populations, to more reliably answer some of the remaining questions pertaining to the EAT.

If results from further studies on the EAT allow and warrant it, a future integration into clinical applications, if not of the model itself, then of the techniques employed, is on the horizon of possibilities. Given that cardiac CT diagnostics is a fast-growing field with expanding clinical potential, any method, which improves image-based risk-stratification beyond calcium scoring or present plaque-analysis models, could become an important tool with great impact on the management of preventive measures at population level.

ACKNOWLEDGEMENTS

The financial support from **Region Västra Götaland** within the framework of the ALF-system, multiple grants received from the **Gothenburg Society of Medicine** (Göteborgs Läkaresällskap), and grants from the **Sahlgrenska University Hospital Research Foundation** have all been essential for my work on the thesis.

The support from the **Sahlgrenska University Hospital**, and more specifically, the **Department of Thoracic Radiology**, has been indispensable. My heartfelt thanks especially to: **Jenny Vikgren**, head of the department for many years, and **Caroline Sandahl Molinder**, current head of the department, who have been generous both with time off from clinical duties and unwavering moral support for my academic efforts.

Had it not been for my colleague **Rauni Rossi Norrlund**, who first gave me the idea, I might never have embarked on this project. She knew that I had an interest in science, more specifically in image analysis, and pleaded with me to contact Professor **Göran Bergström**… And the way it turned out, I'm grateful for the opportunity I was given to be part of his team. Göran Bergström is without any doubt the single person, who has contributed the most to my journey, both as a fellow researcher, supervisor and as the person organizing the various aspects of the work. A role model scientifically, superbly conscientious, always looking forward, he has inspired me with his seemingly inextinguishable curiosity.

As my assistant supervisors over the course of the project, I want to thank professor **Fredrik Kahl**, who opened the door, at least a little, to the world of mathematics, **Ola Hjelmgren**, who has greatly contributed to the technical development of the final analytical model, both conceptually and administratively, **Åse A. Johnsson**, who has given me invaluable moral support and helped me navigate the strange paths of the academic world, and, last but not least, **John Brandberg**, whose practical and clear-sighted view in research is commendable, and who, ever since he became the head of the Department of Radiology at the Sahlgrenska University Hospital, has maintained his strong support of the project.

All my fellow researchers deserve to be equally lauded for their hard work and their unassuming, generous attitude. The initial, technical work owes much to

Alexander Norlén and **Jennifer Alvén**, who under the supervision of Fredrik Kahl and **Olof Enqvist** developed important aspects of the methodology. Olof Enqvist and later **Johannes Ulén** and **Måns Larsson** have contributed immensely to the development of the analytical model and its further improvements. **Elias Björnson** has generously helped me to overcome many hurdles in the field of statistics, always ready to come to the rescue, and has together with **Martin Adiels** contributed greatly to the analysis of our data. Professor **Fredrik Bäckhed**, Professor **Lennart Bergfeldt** and **Anders Gummesson** have all shared their vast knowledge and helped me to improve the manuscripts beyond the limits of my own shortcomings. **Helén Milde** and **Marit Johannesson** have generously shared their know-how and experience in the field of computed tomography, whenever I had questions related to image acquisition. **Sven-Göran Johansson** and **Tiffany Hurtig** have been more than helpful with computers and all kinds of IT-related support during the project.

Finally, a gigantic thumbs up to **all my colleagues and co-workers** both at the Department of Thoracic Radiology and the Department of Nuclear Medicine, who have exhibited both tolerance, patience and understanding. Without your supporting attitude, the project would have been if not impossible, inhumanely tough to finish.

REFERENCES

1. Rodriguez, E. R. & Tan, C. D. Structure and Anatomy of the Human Pericardium. *Progress in Cardiovascular Diseases* vol. 59 Preprint at https://doi.org/10.1016/j.pcad.2016.12.010 (2017).

2. Sacks, H. S. & Fain, J. N. Human epicardial adipose tissue: A review. *American Heart Journal* vol. 153 Preprint at https://doi.org/10.1016/j.ahj.2007.03.019 (2007).

3. Madonna, R., Massaro, M., Scoditti, E., Pescetelli, I. & De Caterina, R. The epicardial adipose tissue and the coronary arteries: dangerous liaisons. *Cardiovasc Res* **115**, 1013–1025 (2019).

4. Iacobellis, G. & Bianco, A. C. Epicardial adipose tissue: emerging physiological, pathophysiological and clinical features. *Trends Endocrinol Metab* **22**, 450–457 (2011).

5. Iacobellis, G. Epicardial adipose tissue in contemporary cardiology. *Nature Reviews Cardiology* vol. 19 Preprint at https://doi.org/10.1038/s41569-022-00679-9 (2022).

6. Mazurek, T. *et al.* Human Epicardial Adipose Tissue Is a Source of Inflammatory Mediators. *Circulation* **108**, (2003).

7. Konwerski, M., Gasecka, A., Opolski, G., Grabowski, M. & Mazurek, T. Role of Epicardial Adipose Tissue in Cardiovascular Diseases: A Review. *Biology* vol. 11 Preprint at https://doi.org/10.3390/biology11030355 (2022).

8. Kitagawa, T. *et al.* The relationship between inflammation and neoangiogenesis of epicardial adipose tissue and coronary atherosclerosis based on computed tomography analysis. *Atherosclerosis* **243**, 293–299 (2015).

9. Nerlekar, N. *et al.* The Natural history of Epicardial Adipose Tissue Volume and Attenuation: A long-term prospective cohort follow-up study. *Sci Rep* **10**, (2020).

10. El Khoudary, S. R. *et al.* Effects of Hormone Therapy on Heart Fat and Coronary Artery Calcification Progression: Secondary Analysis From the KEEPS Trial. *J Am Heart Assoc* **8**, (2019).

11. Raggi, P. *et al.* Statins Reduce Epicardial Adipose Tissue Attenuation Independent of Lipid Lowering: A Potential Pleiotropic Effect. *J Am Heart Assoc* **8**, (2019).

12. Patel, V. B., Shah, S., Verma, S. & Oudit, G. Y. Epicardial adipose tissue as a metabolic transducer: role in heart failure and coronary artery disease. *Heart Failure Reviews* vol. 22 Preprint at https://doi.org/10.1007/s10741-017-9644-1 (2017).

13. Nerlekar, N. *et al.* Association of Epicardial Adipose Tissue and High-Risk Plaque Characteristics: A Systematic Review and Meta-Analysis. *J Am Heart Assoc* **6**, (2017).

14. Mancio, J. *et al.* Epicardial adipose tissue volume assessed by computed tomography and coronary artery disease: a systematic review and meta-analysis. *Eur Heart J Cardiovasc Imaging* (2017) doi:10.1093/ehjci/jex314.

15. Chong, B. *et al.* Epicardial Adipose Tissue Assessed by Computed Tomography and Echocardiography Are Associated with Adverse Cardiovascular Outcomes: A Systematic Review and Meta-Analysis. *Circ Cardiovasc Imaging* **16**, (2023).

16. Christensen, R. H., von Scholten, B. J., Lehrskov, L. L., Rossing, P. & Jorgensen, P. G. Epicardial adipose tissue: an emerging biomarker of cardiovascular complications in type 2 diabetes? *Ther Adv Endocrinol Metab* **11**, 2042018820928824 (2020).

17. Li, Y. *et al.* Epicardial fat tissue in patients with diabetes mellitus: A systematic review and meta-analysis. *Cardiovascular Diabetology* vol. 18 Preprint at https://doi.org/10.1186/s12933-019-0807-3 (2019).

18. Archer, J. M. *et al.* Season and clinical factors influence epicardial adipose tissue attenuation measurement on computed tomography and may hamper its utilization as a risk marker. *Atherosclerosis* **321**, 8–13 (2021).

19. Zoico, E. *et al.* Brown and beige adipose tissue and aging. *Front Endocrinol (Lausanne)* **10**, (2019).

20. Iacobellis, G. & Mahabadi, A. A. Is epicardial fat attenuation a novel marker of coronary inflammation? *Atherosclerosis* **284**, 212–213 (2019).

21. Marwan, M. *et al.* CT Attenuation of Pericoronary Adipose Tissue in Normal Versus Atherosclerotic Coronary Segments as Defined by Intravascular Ultrasound. *J Comput Assist Tomogr* **41**, 762–767 (2017).

22. Chen, X. *et al.* Pericoronary adipose tissue attenuation assessed by dual-layer spectral detector computed tomography is a sensitive imaging marker of high-risk plaques. *Quant Imaging Med Surg* **11**, 2093–2103 (2021).

23. Milanese, G. *et al.* Quantification of epicardial fat with cardiac CT angiography and association with cardiovascular risk factors in symptomatic patients: From the ALTER-BIO (alternative cardiovascular bio-imaging markers) registry. *Diagnostic and Interventional Radiology* **25**, (2019).

24. Lin, A. *et al.* Metabolic syndrome, fatty liver, and artificial intelligence-based epicardial adipose tissue measures predict long-term risk of cardiac events: a prospective study. *Cardiovasc Diabetol* **20**, (2021).

25. Nerlekar, N. *et al.* Poor Correlation, Reproducibility, and Agreement Between Volumetric Versus Linear Epicardial Adipose Tissue Measurement: A 3D Computed Tomography Versus 2D Echocardiography Comparison. *JACC Cardiovasc Imaging* **11**, 1035–1036 (2018).

26. Ohnesorge, B. *et al.* Reproducibility of coronary calcium quantification in repeat examinations with retrospectively ECG-gated multisection spiral CT. *Eur Radiol* **12**, 1532–1540 (2002).

27. Kroft, L. J. M., de Roos, A. & Geleijns, J. Artifacts in ECG-Synchronized MDCT Coronary Angiography. *American Journal of Roentgenology* **189**, 581–591 (2007).

28. Sun, Z. & Ng, K. H. Prospective versus retrospective ECG-gated multislice CT coronary angiography: A systematic review of radiation dose and diagnostic accuracy. *European Journal of Radiology* vol. 81 Preprint at https://doi.org/10.1016/j.ejrad.2011.01.070 (2012).

29. Toia, P. *et al.* Technical development in cardiac CT: Current standards and future improvements—a narrative review. *Cardiovascular Diagnosis and Therapy* vol. 10 Preprint at https://doi.org/10.21037/cdt-20-527 (2020).

30. Hedgire, S. S., Baliyan, V., Ghoshhajra, B. B. & Kalra, M. K. Recent advances in cardiac computed tomography dose reduction strategies: a review of scientific evidence and technical developments. *Journal of Medical Imaging* **4**, (2017).

31. Baron, K. B., Choi, A. D. & Chen, M. Y. Low Radiation Dose Calcium Scoring: Evidence and Techniques. *Current Cardiovascular Imaging Reports* vol. 9 Preprint at https://doi.org/10.1007/s12410-016-9373-1 (2016).

32. Counseller, Q. & Aboelkassem, Y. Recent technologies in cardiac imaging. *Frontiers in Medical Technology* vol. 4 Preprint at https://doi.org/10.3389/fmedt.2022.984492 (2022).

33. Centonze, M. *et al.* Cardiac-CT and cardiac-MR cost-effectiveness: a literature review. *Radiologia Medica* vol. 125 Preprint at https://doi.org/10.1007/s11547-020-01290-z (2020).

34. Mazurek, T. *et al.* Inflammatory capacity of pericoronary adipose tissue among overweight patients with stable angina affects atherosclerotic leasions formation. *Eur Heart J* **34**, (2013).

35. Mazurek, T. *et al.* PET/CT evaluation of 18F-FDG uptake in pericoronary adipose tissue in patients with stable coronary artery disease: Independent predictor of atherosclerotic lesions' formation? *Journal of Nuclear Cardiology* **24**, (2017).

36. Kwiecinski, J. *et al.* Machine Learning with 18F-Sodium Fluoride PET and Quantitative Plaque Analysis on CT Angiography for the Future Risk of Myocardial Infarction. *Journal of Nuclear Medicine* **63**, (2022).

37. Kwiecinski, J. *et al.* Coronary 18F-Sodium Fluoride Uptake Predicts Outcomes in Patients With Coronary Artery Disease. *J Am Coll Cardiol* **75**, (2020).

38. Høilund-Carlsen, P. F., Sturek, M., Alavi, A. & Gerke, O. Atherosclerosis imaging with 18F-sodium fluoride PET: state-of-the-art review. *European Journal of Nuclear Medicine and Molecular Imaging* vol. 47 Preprint at https://doi.org/10.1007/s00259-019-04603-1 (2020).

39. Jukema, R. *et al.* Warranty period of coronary computed tomography angiography and [15O]H2O positron emission tomography in symptomatic patients. *Eur Heart J Cardiovasc Imaging* **24**, (2023).

40. Uusitalo, V. *et al.* The association between coronary flow reserve and development of coronary calcifications: a follow-up study for 11 years in healthy young men. *Eur Heart J Cardiovasc Imaging* **14**, (2013).

41. Danad, I. *et al.* Quantitative assessment of myocardial perfusion in the detection of significant coronary artery disease: Cutoff values and diagnostic accuracy of quantitative [15O]H2O PET imaging. *J Am Coll Cardiol* **64**, (2014).

42. Driessen, R. S. *et al.* Effect of Plaque Burden and Morphology on Myocardial Blood Flow and Fractional Flow Reserve. *J Am Coll Cardiol* **71**, (2018).

43. Driessen, R. S. *et al.* Incremental prognostic value of hybrid [15O]H2O positron emission tomography-computed tomography: Combiningmyocardial blood flow, coronary stenosis severity, and high-risk plaque morphology. *Eur Heart J Cardiovasc Imaging* **21**, (2020).

44. Kaushik, A. *et al.* Estimation of radiation dose to patients from 18FDG whole body PET/CT investigations using dynamic PET scan protocol. *Indian Journal of Medical Research* **142**, (2015).

45. Agatston, A. S. *et al.* Quantification of coronary artery calcium using ultrafast computed tomography. *J Am Coll Cardiol* **15**, 827–832 (1990).

46. Almeida, S. *et al.* Feasibility of measuring pericoronary fat from precontrast scans: Effect of iodinated contrast on pericoronary fat attenuation. *J Cardiovasc Comput Tomogr* **14**, (2020).

47. Seeram, E. Computed tomography: Physical principles and recent technical advances. *J Med Imaging Radiat Sci* **41**, (2010).

48. McCollough, C. H., Leng, S., Yu, L. & Fletcher, J. G. Dual- and multi-energy CT: Principles, technical approaches, and clinical applications. *Radiology* **276**, (2015).

49. Tortora, M. *et al.* Spectral Photon-Counting Computed Tomography: A Review on Technical Principles and Clinical Applications. *Journal of Imaging* vol. 8 Preprint at https://doi.org/10.3390/jimaging8040112 (2022).

50. Ese, Z. *et al.* Influence of conventional and extended CT scale range on quantification of Hounsfield units of medical implants and metallic objects. *Technisches Messen* **85**, (2018).

51. Brooks, R. A. A quantitative theory of the hounsfield unit and its application to dual energy scanning. *J Comput Assist Tomogr* **1**, (1977).

52. Goldman, L. W. Principles of CT: Multislice CT. *Journal of Nuclear Medicine Technology* vol. 36 Preprint at https://doi.org/10.2967/jnmt.107.044826 (2008).

53. Goldman, L. W. Principles of CT and CT technology. *Journal of Nuclear Medicine Technology* vol. 35 Preprint at https://doi.org/10.2967/jnmt.107.042978 (2007).

54. Kang, E. J. Clinical applications of wide-detector CT scanners for cardiothoracic imaging: An update. *Korean Journal of Radiology* vol. 20 Preprint at https://doi.org/10.3348/kjr.2019.0327 (2019).

55. Choi, S. Il *et al.* Recent developments in wide-detector cardiac computed tomography. *International Journal of Cardiovascular Imaging* vol. 25 Preprint at https://doi.org/10.1007/s10554-009-9443-4 (2009).

56. Murayama, K. *et al.* Visualization of lenticulostriate arteries on CT angiography using ultra-high-resolution CT compared with conventional-detector CT. *American Journal of Neuroradiology* **41**, (2020).

57. Ogawa, K. *et al.* Visualization of small visceral arteries on abdominal CT angiography using ultra-high-resolution CT scanner. *Jpn J Radiol* **39**, (2021).

58. Quiney, H. M., Peele, A. G., Gai, Z., Paterson, D. & Nugent, K. A. Diffractive imaging of highly focused X-ray fields. *Nat Phys* **2**, (2006).

59. Keller, O. On the theory of spatial localization of photons. *Physics Reports* vol. 411 Preprint at https://doi.org/10.1016/j.physrep.2005.01.002 (2005).

60. Schuijf, J. D. *et al.* CT imaging with ultra-high-resolution: Opportunities for cardiovascular imaging in clinical practice. *Journal of Cardiovascular Computed Tomography* vol. 16 Preprint at https://doi.org/10.1016/j.jcct.2022.02.003 (2022).

61. Kawashima, H. *et al.* Technical Note: Performance comparison of ultra-high-resolution scan modes of two clinical computed tomography systems. *Med Phys* **47**, (2020).

62. Wang, J. & Fleischmann, D. Improving spatial resolution at CT: Development, benefits, and pitfalls. *Radiology* vol. 289 Preprint at https://doi.org/10.1148/radiol.2018181156 (2018).

63. Hata, A. *et al.* Effect of Matrix Size on the Image Quality of Ultra-high-resolution CT of the Lung. *Acad Radiol* **25**, (2018).

64. Rajendran, K. *et al.* First Clinical Photon-counting Detector CT System: Technical Evaluation. *Radiology* **303**, (2022).

65. Zhou, W. *et al.* Comparison of a photon-counting-detector CT with an energy-integrating-detector CT for temporal bone imaging: A cadaveric study. *American Journal of Neuroradiology* **39**, (2018).

66. Flohr, T. *et al.* Photon-counting CT review. *Physica Medica* vol. 79 Preprint at https://doi.org/10.1016/j.ejmp.2020.10.030 (2020).

67. Doukbi, E. *et al.* Browning Epicardial Adipose Tissue: Friend or Foe? *Cells* vol. 11 Preprint at https://doi.org/10.3390/cells11060991 (2022).

68. Sjostrom, L., Kvist, H., Cederblad, A. & Tylen, U. Determination of total adipose tissue and body fat in women by computed tomography, 40K, and tritium. *Am J Physiol* **250**, E736-45 (1986).

69. Ferland, M. *et al.* Assessment of adipose tissue distribution by computed axial tomography in obese women: association with body density and anthropometric measurements. *British Journal of Nutrition* **61**, (1989).

70. A Review on Morphological Filter and its Implementation. *International Journal of Science and Research (IJSR)* **6**, (2017).

71. Wheeler, G. L. *et al.* Pericardial and visceral adipose tissues measured volumetrically with computed tomography are highly associated in type 2 diabetic families. *Invest Radiol* **40**, 97–101 (2005).

72. Rosito, G. A. *et al.* Pericardial fat, visceral abdominal fat, cardiovascular disease risk factors, and vascular calcification in a community-based sample: the Framingham Heart Study. *Circulation* **117**, 605–613 (2008).

73. Mahabadi, A. A. *et al.* Association of epicardial fat with cardiovascular risk factors and incident myocardial infarction in the general population: The Heinz Nixdorf recall study. *J Am Coll Cardiol* **61**, 1388–1395 (2013).

74. Forouzandeh, F. *et al.* Does quantifying epicardial and intrathoracic fat with noncontrast computed tomography improve risk stratification beyond calcium scoring alone? *Circ Cardiovasc Imaging* **6**, (2013).

75. Britton, K. A. *et al.* Body fat distribution, incident cardiovascular disease, cancer, and all-cause mortality. *J Am Coll Cardiol* **62**, (2013).

76. Kunita, E. *et al.* Prognostic value of coronary artery calcium and epicardial adipose tissue assessed by non-contrast cardiac computed tomography. *Atherosclerosis* **233**, (2014).

77. Militello, C. *et al.* A semi-automatic approach for epicardial adipose tissue segmentation and quantification on cardiac CT scans. *Comput Biol Med* **114**, 103424 (2019).

78. Ni, J. *et al.* A survey on theories and applications for self-driving cars based on deep learning methods. *Applied Sciences (Switzerland)* vol. 10 Preprint at https://doi.org/10.3390/APP10082749 (2020).

79. Zahradnikova, B., Duchovicova, S. & Schreiber, P. Image Mining: Review and New Challenges. *International Journal of Advanced Computer Science and Applications* **6**, (2015).

80. Li, Z. *et al.* Cloud and cloud shadow detection for optical satellite imagery: Features, algorithms, validation, and prospects. *ISPRS Journal of Photogrammetry and Remote Sensing* vol. 188 Preprint at https://doi.org/10.1016/j.isprsjprs.2022.03.020 (2022).

81. Nti, I. K., Adekoya, A. F., Weyori, B. A. & Nyarko-Boateng, O. Applications of artificial intelligence in engineering and manufacturing: a systematic review. *Journal of Intelligent Manufacturing* vol. 33 Preprint at https://doi.org/10.1007/s10845-021-01771-6 (2022).

82. Ahmad, H. MACHINE LEARNING APPLICATIONS IN OCEANOGRAPHY. *Aquatic Research* (2019) doi:10.3153/ar19014.

83. Shahzad, R. *et al.* Automatic quantification of epicardial fat volume on non-enhanced cardiac CT scans using a multi-atlas segmentation approach. *Med Phys* **40**, 91910 (2013).

84. Rodrigues, E. O. *et al.* A novel approach for the automated segmentation and volume quantification of cardiac fats on computed tomography. *Comput Methods Programs Biomed* **123**, 109–128 (2016).

85. Norlen, A. *et al.* Automatic pericardium segmentation and quantification of epicardial fat from computed tomography angiography. *J Med Imaging (Bellingham)* **3**, 34003 (2016).

86. Ding, X. *et al.* Automated pericardium delineation and epicardial fat volume quantification from noncontrast CT. *Med Phys* **42**, 5015–5026 (2015).

87. Kirisli, H. A. *et al.* Fully automatic cardiac segmentation from 3D CTA data: a multi-atlas based approach. in *Medical Imaging 2010: Image Processing* vol. 7623 (2010).

88. Dey, D. *et al.* Automated algorithm for atlas-based segmentation of the heart and pericardium from non-contrast CT. in *Medical Imaging 2010: Image Processing* vol. 7623 (2010).

89. Spearman, J. V *et al.* Automated quantification of epicardial adipose tissue using CT angiography: evaluation of a prototype software. *Eur Radiol* **24**, 519–526 (2014).

90. Iglesias, J. E. & Sabuncu, M. R. Multi-atlas segmentation of biomedical images: A survey. *Med Image Anal* **24**, (2015).

91. Tufail, S., Riggs, H., Tariq, M. & Sarwat, A. I. Advancements and Challenges in Machine Learning: A Comprehensive Review of Models, Libraries, Applications, and Algorithms. *Electronics (Switzerland)* vol. 12 Preprint at https://doi.org/10.3390/electronics12081789 (2023).

92. Waring, J., Lindvall, C. & Umeton, R. Automated machine learning: Review of the state-of-the-art and opportunities for healthcare. *Artificial Intelligence in Medicine* vol. 104 Preprint at https://doi.org/10.1016/j.artmed.2020.101822 (2020).

93. Dhillon, A. & Verma, G. K. Convolutional neural network: a review of models, methodologies and applications to object detection. *Progress in Artificial Intelligence* vol. 9 Preprint at https://doi.org/10.1007/s13748-019-00203-0 (2020).

94. Tajbakhsh, N. *et al.* Embracing imperfect datasets: A review of deep learning solutions for medical image segmentation. *Med Image Anal* **63**, (2020).

95. Commandeur, F. *et al.* Deep Learning for Quantification of Epicardial and Thoracic Adipose Tissue From Non-Contrast CT. *IEEE Trans Med Imaging* **37**, 1835–1846 (2018).

96. He, X. *et al.* Automatic segmentation and quantification of epicardial adipose tissue from coronary computed tomography angiography. *Phys Med Biol* **65**, (2020).

97. Liu, L. *et al.* The U-Net Family for Epicardial Adipose Tissue Segmentation and Quantification in Low-Dose CT. *Technologies (Basel)* **11**, (2023).

98. Qu, J. *et al.* Deep Learning-Based Approach for the Automatic Quantification of Epicardial Adipose Tissue from Non-Contrast CT. *Cognit Comput* **14**, (2022).

99. West, H. W. *et al.* Deep-Learning for Epicardial Adipose Tissue Assessment With Computed Tomography: Implications for Cardiovascular Risk Prediction. *JACC Cardiovasc Imaging* **16**, (2023).

100. Eggen, D. A., Strong, J. P. & McGill H. C., Jr. Coronary calcification. Relationship to clinically significant coronary lesions and race, sex, and topographic distribution. *Circulation* **32**, 948–955 (1965).

101. Otsuka, F., Sakakura, K., Yahagi, K., Joner, M. & Virmani, R. Has our understanding of calcification in human coronary atherosclerosis progressed? *Arterioscler Thromb Vasc Biol* **34**, (2014).

102. Andrews, J., Psaltis, P. J., Bartolo, B. A. D., Nicholls, S. J. & Puri, R. Coronary arterial calcification: A review of mechanisms, promoters and imaging. *Trends in Cardiovascular Medicine* vol. 28 Preprint at https://doi.org/10.1016/j.tcm.2018.04.007 (2018).

103. Johnson, R. C., Leopold, J. A. & Loscalzo, J. Vascular calcification: Pathobiological mechanisms and clinical implications. *Circulation Research* vol. 99 Preprint at https://doi.org/10.1161/01.RES.0000249379.55535.21 (2006).

104. You, A. Y. F. *et al.* Raman spectroscopy imaging reveals interplay between atherosclerosis and medial calcification in the human aorta. *Sci Adv* **3**, (2017).

105. Homorodean, C. *et al.* Intravascular ultrasound insights into the unstable features of the coronary atherosclerotic plaques: A systematic review and meta-analysis. *European Journal of Clinical Investigation* vol. 52 Preprint at https://doi.org/10.1111/eci.13671 (2022).

106. Mintz, G. S. Intravascular imaging of coronary calcification and its clinical implications. *JACC: Cardiovascular Imaging* vol. 8 Preprint at https://doi.org/10.1016/j.jcmg.2015.02.003 (2015).

107. Ono, M. *et al.* Advances in IVUS/OCT and Future Clinical Perspective of Novel Hybrid Catheter System in Coronary Imaging. *Frontiers in Cardiovascular Medicine* vol. 7 Preprint at https://doi.org/10.3389/fcvm.2020.00119 (2020).

108. Araki, M. *et al.* Optical coherence tomography in coronary atherosclerosis assessment and intervention. *Nature Reviews Cardiology* vol. 19 Preprint at https://doi.org/10.1038/s41569-022-00687-9 (2022).

109. Ehara, S. *et al.* Spotty calcification typifies the culprit plaque in patients with acute myocardial infarction: an intravascular ultrasound study. *Circulation* **110**, 3424–3429 (2004).

110. van Velzen, J. E. *et al.* Comprehensive assessment of spotty calcifications on computed tomography angiography: comparison to plaque characteristics on intravascular ultrasound with radiofrequency backscatter analysis. *J Nucl Cardiol* **18**, 893–903 (2011).

111. Ito, T. *et al.* Impact of epicardial fat volume on coronary artery disease in symptomatic patients with a zero calcium score. *Int J Cardiol* **167**, (2013).

112. Meijs, M. F. L. *et al.* Comparison of Frequency of Calcified Versus Non-Calcified Coronary Lesions by Computed Tomographic Angiography in Patients With Stable Versus Unstable Angina Pectoris. *Am J Cardiol* **104**, 305–311 (2009).

113. Oka, T. *et al.* Association between epicardial adipose tissue volume and characteristics of non-calcified plaques assessed by coronary computed tomographic angiography. *Int J Cardiol* **161**, 45–49 (2012).

114. Hwang, I. C., Park, H. E. & Choi, S. Y. Epicardial Adipose Tissue Contributes to the Development of Non-Calcified Coronary Plaque: A 5-Year Computed Tomography Follow-up Study. *J Atheroscler Thromb* **24**, 262–274 (2017).

115. Meijs, M. F. L. *et al.* Comparison of Frequency of Calcified Versus Non-Calcified Coronary Lesions by Computed Tomographic Angiography in Patients With Stable Versus Unstable Angina Pectoris. *Am J Cardiol* **104**, 305–311 (2009).

116. Tam, L. M. *et al.* Absolute coronary artery calcium score is the best predictor of non-calcified plaque involvement in patients with low calcium scores (1-100). *Atherosclerosis* **230**, 76–79 (2013).

117. Alexopoulos, N. *et al.* EPICARDIAL ADIPOSE TISSUE AND CORONARY ARTERY PLAQUE CHARACTERISTICS. *J Am Coll Cardiol* **55**, (2010).

118. Konen, E. *et al.* The prevalence and anatomical patterns of intramuscular coronary arteries: a coronary computed tomography angiographic study. *J Am Coll Cardiol* **49**, 587–593 (2007).

119. Hirata, Y. *et al.* Enhanced inflammation in epicardial fat in patients with coronary artery disease. *Int Heart J* **52**, 139–142 (2011).

120. Kitagawa, T. *et al.* The relationship between inflammation and neoangiogenesis of epicardial adipose tissue and coronary atherosclerosis based on computed tomography analysis. *Atherosclerosis* **243**, 293–299 (2015).

121. Hajsadeghi, F. *et al.* Increased epicardial adipose tissue is associated with coronary artery disease and major adverse cardiovascular events. *Atherosclerosis* **237**, 486–489 (2014).

122. Eisenberg, E. *et al.* Deep Learning-Based Quantification of Epicardial Adipose Tissue Volume and Attenuation Predicts Major Adverse Cardiovascular Events in Asymptomatic Subjects. *Circ Cardiovasc Imaging* (2020) doi:10.1161/CIRCIMAGING.119.009829.

123. Commandeur, F. *et al.* Machine learning to predict the long-term risk of myocardial infarction and cardiac death based on clinical risk, coronary calcium, and epicardial adipose tissue: a prospective study. *Cardiovasc Res* **116**, 2216–2225 (2020).

124. Villasante Fricke, A. C. & Iacobellis, G. Epicardial Adipose Tissue: Clinical Biomarker of Cardio-Metabolic Risk. *International journal of*

molecular sciences vol. 20 Preprint at https://doi.org/10.3390/ijms20235989 (2019).

125. Ding, J. *et al.* The association of pericardial fat with incident coronary heart disease: the Multi-Ethnic Study of Atherosclerosis (MESA). *Am J Clin Nutr* **90**, 499–504 (2009).

126. de Vos, A. M. *et al.* Peri-coronary epicardial adipose tissue is related to cardiovascular risk factors and coronary artery calcification in post-menopausal women. *Eur Heart J* **29**, 777–783 (2008).

127. Wang, T. D. *et al.* Association of epicardial adipose tissue with coronary atherosclerosis is region-specific and independent of conventional risk factors and intra-abdominal adiposity. *Atherosclerosis* **213**, 279–287 (2010).

128. Fitzgibbons, T. P. *et al.* Coronary disease is not associated with robust alterations in inflammatory gene expression in human epicardial fat. *JCI Insight* **4**, (2019).

129. Chen, Y. C. *et al.* Epicardial adipose tissue thickness is not associated with adverse cardiovascular events in patients undergoing haemodialysis. *Sci Rep* **10**, (2020).

130. Mancio, J. *et al.* Epicardial adipose tissue volume assessed by computed tomography and coronary artery disease: a systematic review and meta-analysis. *Eur Heart J Cardiovasc Imaging* (2017) doi:10.1093/ehjci/jex314.

131. Marwan, M. *et al.* CT Attenuation of Pericoronary Adipose Tissue in Normal Versus Atherosclerotic Coronary Segments as Defined by Intravascular Ultrasound. *J Comput Assist Tomogr* **41**, 762–767 (2017).

132. Achenbach, S. *et al.* Detection of calcified and noncalcified coronary atherosclerotic plaque by contrast-enhanced, submillimeter multidetector spiral computed tomography: a segment-based comparison with intravascular ultrasound. *Circulation* **109**, 14–17 (2004).

133. Kawasaki, M. *et al.* Diagnostic Accuracy of Optical Coherence Tomography and Integrated Backscatter Intravascular Ultrasound

Images for Tissue Characterization of Human Coronary Plaques. *J Am Coll Cardiol* **48**, (2006).

134. Takahashi, T. *et al.* Diagnostic performance of fractional flow reserve derived from coronary angiography, intravascular ultrasound, and optical coherence tomography; a meta-analysis. *J Cardiol* **80**, (2022).

135. Papadopoulou, S. L. *et al.* Detection and quantification of coronary atherosclerotic plaque by 64-slice multidetector CT: a systematic head-to-head comparison with intravascular ultrasound. *Atherosclerosis* **219**, 163–170 (2011).

136. Papadopoulou, S. L. *et al.* Detection and quantification of coronary atherosclerotic plaque by 64-slice multidetector CT: a systematic head-to-head comparison with intravascular ultrasound. *Atherosclerosis* **219**, 163–170 (2011).

137. Lin, A. *et al.* Pericoronary adipose tissue computed tomography attenuation distinguishes different stages of coronary artery disease: a cross-sectional study. *Eur Heart J Cardiovasc Imaging* **22**, 298–306 (2021).

138. Park, H. B. *et al.* Clinical Feasibility of 3D Automated Coronary Atherosclerotic Plaque Quantification Algorithm on Coronary Computed Tomography Angiography: Comparison with Intravascular Ultrasound. *Eur Radiol* **25**, 3073–3083 (2015).

139. Eisenberg, E. *et al.* Deep Learning-Based Quantification of Epicardial Adipose Tissue Volume and Attenuation Predicts Major Adverse Cardiovascular Events in Asymptomatic Subjects. *Circ Cardiovasc Imaging* (2020) doi:10.1161/CIRCIMAGING.119.009829.

140. Lu, M. T. *et al.* Epicardial and paracardial adipose tissue volume and attenuation - Association with high-risk coronary plaque on computed tomographic angiography in the ROMICAT II trial. *Atherosclerosis* **251**, 47–54 (2016).

141. Commandeur, F. *et al.* Fully Automated CT Quantification of Epicardial Adipose Tissue by Deep Learning: A Multicenter Study. *Radiol Artif Intell* **1**, e190045 (2019).

142. Marwan, M. *et al.* Quantification of epicardial adipose tissue by cardiac CT: Influence of acquisition parameters and contrast enhancement. *Eur J Radiol* **121**, 108732 (2019).

143. Mancio, J. *et al.* Epicardial adipose tissue volume and annexin A2/fetuin-A signalling are linked to coronary calcification in advanced coronary artery disease: Computed tomography and proteomic biomarkers from the EPICHEART study. *Atherosclerosis* **292**, 75–83 (2020).

144. Milanese, G. *et al.* Validity of epicardial fat volume as biomarker of coronary artery disease in symptomatic individuals: Results from the ALTER-BIO registry. *Int J Cardiol* **314**, 20–24 (2020).

145. Sacks, H. S. *et al.* Adult epicardial fat exhibits beige features. *Journal of Clinical Endocrinology and Metabolism* **98**, (2013).

146. Packer, M. Epicardial Adipose Tissue May Mediate Deleterious Effects of Obesity and Inflammation on the Myocardium. *Journal of the American College of Cardiology* vol. 71 Preprint at https://doi.org/10.1016/j.jacc.2018.03.509 (2018).

147. Cherian, S., Lopaschuk, G. D. & Carvalho, E. Cellular cross-talk between epicardial adipose tissue and myocardium in relation to the pathogenesis of cardiovascular disease. *American Journal of Physiology - Endocrinology and Metabolism* vol. 303 Preprint at https://doi.org/10.1152/ajpendo.00061.2012 (2012).

148. Manco, M. *et al.* Epicardial fat, abdominal adiposity and insulin resistance in obese pre-pubertal and early pubertal children. *Atherosclerosis* **226**, 490–495 (2013).

149. Rabkin, S. W. The relationship between epicardial fat and indices of obesity and the metabolic syndrome: a systematic review and meta-analysis. *Metab Syndr Relat Disord* **12**, 31–42 (2014).

150. Gorter, P. M. *et al.* Quantification of epicardial and peri-coronary fat using cardiac computed tomography; reproducibility and relation with obesity and metabolic syndrome in patients suspected of coronary artery disease. *Atherosclerosis* **197**, 896–903 (2008).

151. Bakkum, M. J. *et al.* The impact of obesity on the relationship between epicardial adipose tissue, left ventricular mass and coronary microvascular function. *Eur J Nucl Med Mol Imaging* **42**, 1562–1573 (2015).

152. Rabkin, S. W. Epicardial fat: properties, function and relationship to obesity. *Obes Rev* **8**, 253–261 (2007).

153. Jayedi, A. *et al.* Anthropometric and adiposity indicators and risk of type 2 diabetes: systematic review and dose-response meta-analysis of cohort studies. *The BMJ* vol. 376 Preprint at https://doi.org/10.1136/bmj-2021-067516 (2022).

154. Morris, D. H. *et al.* Progression rates from HbA1c 6.0-6.4% and other prediabetes definitions to type 2 diabetes: a meta-analysis. *Diabetologia* **56**, 1489–1493 (2013).

155. Abdul-Ghani, M., Defronzo, R. A. & Jayyousi, A. Prediabetes and risk of diabetes and associated complications: Impaired fasting glucose versus impaired glucose tolerance: does it matter? *Curr Opin Clin Nutr Metab Care* **19**, 394–399 (2016).

156. Neeland, I. J. *et al.* Dysfunctional adiposity and the risk of prediabetes and type 2 diabetes in obese adults. *JAMA* **308**, 1150–1159 (2012).

157. Guasch-Ferre, M. *et al.* Metabolomics in Prediabetes and Diabetes: A Systematic Review and Meta-analysis. *Diabetes Care* **39**, 833–846 (2016).

158. Stefan, N., Fritsche, A., Schick, F. & Haring, H. U. Phenotypes of prediabetes and stratification of cardiometabolic risk. *Lancet Diabetes Endocrinol* **4**, 789–798 (2016).

159. Tabák, A. G., Herder, C., Rathmann, W., Brunner, E. J. & Kivimäki, M. Prediabetes: A high-risk state for diabetes development. *The Lancet* **379**, 2279–2290 (2012).

160. Beulens, J. W. J. *et al.* Risk and management of pre-diabetes. *Eur J Prev Cardiol* **26**, (2019).

161. Van Herpt, T. T. W. *et al.* Lifetime risk to progress from pre-diabetes to type 2 diabetes among women and men: Comparison between American Diabetes Association and World Health Organization diagnostic criteria. *BMJ Open Diabetes Res Care* **8**, (2020).

162. Li, N. *et al.* Factors associated with progression of different prediabetic status to Diabetes: A Community-based cohort study. *Diabetes Res Clin Pract* **184**, (2022).

163. Janghorbani, M. & Amini, M. Progression from optimal blood glucose and pre-diabetes to type 2 diabetes in a high risk population with or without hypertension in Isfahan, Iran. *Diabetes Res Clin Pract* **108**, (2015).

164. Meyer, C. *et al.* Different mechanisms for impaired fasting glucose and impaired postprandial glucose tolerance in humans. *Diabetes Care* **29**, (2006).

165. Ha, J. & Sherman, A. Type 2 diabetes: one disease, many pathways. *Am J Physiol Endocrinol Metab* **319**, (2020).

166. Borel, A. L. *et al.* Visceral, subcutaneous abdominal adiposity and liver fat content distribution in normal glucose tolerance, impaired fasting glucose and/or impaired glucose tolerance. *Int J Obes* **39**, (2015).

167. Smith, U. & Kahn, B. B. Adipose tissue regulates insulin sensitivity: role of adipogenesis, de novo lipogenesis and novel lipids. *J Intern Med* **280**, (2016).

168. Sampath Kumar, A. *et al.* Exercise and insulin resistance in type 2 diabetes mellitus: A systematic review and meta-analysis. *Annals of Physical and Rehabilitation Medicine* vol. 62 Preprint at https://doi.org/10.1016/j.rehab.2018.11.001 (2019).

169. Skoglund, G., Nilsson, B. B., Olsen, C. F., Bergland, A. & Hilde, G. Facilitators and barriers for lifestyle change in people with prediabetes: a meta-synthesis of qualitative studies. *BMC Public Health* **22**, (2022).

170. McDermott, J., Rentzepis, P. & Kwon, J. The Prediabetes Diet Plan: How to Reverse Prediabetes and Prevent Diabetes Through Healthy Eating and Exercise. *Clinical Diabetes* **36**, (2018).

171. Wang, S. M. *et al.* Contribution of epicardial and abdominopelvic visceral adipose tissues in Chinese adults with impaired glucose regulation and diabetes. *Acta Diabetol* **56**, (2019).

172. Yang, F. S. *et al.* High pericardial and peri-aortic adipose tissue burden in pre-diabetic and diabetic subjects. *BMC Cardiovasc Disord* **13**, 98 (2013).

173. Versteylen, M. O. *et al.* Epicardial adipose tissue volume as a predictor for coronary artery disease in diabetic, impaired fasting glucose, and non-diabetic patients presenting with chest pain. *Eur Heart J Cardiovasc Imaging* **13**, 517–523 (2012).

174. Wang, C. P. *et al.* Increased epicardial adipose tissue (EAT) volume in type 2 diabetes mellitus and association with metabolic syndrome and severity of coronary atherosclerosis. *Clin Endocrinol (Oxf)* **70**, 876–882 (2009).

175. Chun, H., Suh, E., Byun, A. R., Park, H. R. & Shim, K. W. Epicardial fat thickness is associated to type 2 diabetes mellitus in Korean men: a cross-sectional study. *Cardiovasc Diabetol* **14**, 46 (2015).

176. Groves, E. M. *et al.* Comparison of epicardial adipose tissue volume and coronary artery disease severity in asymptomatic adults with versus without diabetes mellitus. *Am J Cardiol* **114**, 686–691 (2014).

177. Ye, R. Z., Richard, G., Gévry, N., Tchernof, A. & Carpentier, A. C. Fat Cell Size: Measurement Methods, Pathophysiological Origins, and Relationships With Metabolic Dysregulations. *Endocrine Reviews* vol. 43 Preprint at https://doi.org/10.1210/endrev/bnab018 (2022).

178. Muir, L. A. *et al.* Adipose tissue fibrosis, hypertrophy, and hyperplasia: Correlations with diabetes in human obesity. *Obesity* **24**, (2016).

179. Molnar, D. *et al.* Pre-diabetes is associated with attenuation rather than volume of epicardial adipose tissue on computed tomography. *Sci Rep* **13**, 1623 (2023).

180. Ferrannini, E., Gastaldelli, A. & Iozzo, P. Pathophysiology of Prediabetes. *Medical Clinics of North America* vol. 95 Preprint at https://doi.org/10.1016/j.mcna.2010.11.005 (2011).

181. Meikle, P. J. *et al.* Plasma Lipid Profiling Shows Similar Associations with Prediabetes and Type 2 Diabetes. *PLoS One* **8**, (2013).

182. Mota, M. *et al.* Prevalence of diabetes mellitus and prediabetes in the adult Romanian population: PREDATORR study. *J Diabetes* **8**, (2016).

183. Bhowmik, B. *et al.* Serum lipid profile and its association with diabetes and prediabetes in a rural Bangladeshi population. *Int J Environ Res Public Health* **15**, (2018).

184. Mahabadi, A. A. *et al.* Cardiac computed tomography-derived epicardial fat volume and attenuation independently distinguish patients with and without myocardial infarction. *PLoS One* **12**, e0183514 (2017).

185. Franssens, B. T., Nathoe, H. M., Leiner, T., Van Der Graaf, Y. & Visseren, F. L. J. Relation between cardiovascular disease risk factors and epicardial adipose tissue density on cardiac computed tomography in patients at high risk of cardiovascular events. *Eur J Prev Cardiol* **24**, (2017).

186. Libby, P. & Theroux, P. Pathophysiology of coronary artery disease. *Circulation* vol. 111 Preprint at https://doi.org/10.1161/CIRCULATIONAHA.105.537878 (2005).

187. Cajavilca, C. & Varon, J. Willem Einthoven: The development of the human electrocardiogram. *Resuscitation* **76**, 325–328 (2008).

188. Oehler, A., Feldman, T., Henrikson, C. & Tereshchenko, L. QRS-T Angle: A Review. *Annals of Noninvasive Electrocardiology* **19**, 534–542 (2014).

189. Man, S., Maan, A., Schalij, M. & Swenne, C. Vectorcardiographic diagnostic & prognostic information derived from the 12-lead electrocardiogram: Historical review and clinical perspective. *J Electrocardiol* **48**, 463–475 (2015).

190. Bortolan, G., Christov, I. & Simova, I. Modifications in Electrocardiographic and Vectordardiographic Morphological Parameters in Elderly Males as Result of Cardiovascular Diseases and Diabetes Mellitus. *Diagnostics* **12**, (2022).

191. Čalošević, S., Dinjar, K., Čalošević, S., Kurbel, S. & Steiner, R. Hidden information in three-axial ECG data of normal subjects: Fractal dimensions of corresponding points from successive QRS loops as a potential sport & age dependent marker. *Gen Physiol Biophys* **35**, (2016).

192. Beck, S. *et al.* Detection of ECG alterations typical for myocardial ischemia: New methods 2021. *Internist* Preprint at https://doi.org/10.1007/s00108-021-01037-6 (2021).

193. Bergfeldt, L. *et al.* Spatial peak and mean QRS-T angles: A comparison of similar but different emerging risk factors for cardiac death. *J Electrocardiol* **61**, 112–120 (2020).

194. Lingman, M. *et al.* Value of the QRS-T area angle in improving the prediction of sudden cardiac death after acute coronary syndromes. *Int J Cardiol* **218**, 1–11 (2016).

195. Tang, P. T., Shenasa, M. & Boyle, N. G. Ventricular Arrhythmias and Sudden Cardiac Death. *Cardiac Electrophysiology Clinics* vol. 9 Preprint at https://doi.org/10.1016/j.ccep.2017.08.004 (2017).

196. Deyell, M. W., Krahn, A. D. & Goldberger, J. J. Sudden Cardiac Death Risk Stratification. *Circ Res* **116**, (2015).

197. Sara, J. D., Eleid, M. F., Gulati, R. & Holmes, D. R. Sudden cardiac death from the perspective of coronary artery disease. *Mayo Clinic Proceedings* vol. 89 Preprint at https://doi.org/10.1016/j.mayocp.2014.08.022 (2014).

198. Sandstedt, M. *et al.* Wide QRS-T angles are associated with markers of increased inflammatory activity independently of hypertension and diabetes. *Annals of Noninvasive Electrocardiology* **25**, e12781 (2020).

199. Hatem, S. & Sanders, P. Epicardial adipose tissue and atrial fibrillation. *Cardiovasc Res* **102**, 205–213 (2014).

200. Al-Rawahi, M., Proietti, R. & Thanassoulis, G. Pericardial fat and atrial fibrillation: Epidemiology, mechanisms and interventions. *Int J Cardiol* **195**, 98–103 (2015).

201. Zhu, W., Zhang, H., Guo, L. & Hong, K. Relationship between epicardial adipose tissue volume and atrial fibrillation. *Herz* **41**, (2016).

202. Hirata, Y. *et al.* Enhanced inflammation in epicardial fat in patients with coronary artery disease. *Int Heart J* **52**, 139–142 (2011).

203. Lin, A. *et al.* Pericoronary adipose tissue computed tomography attenuation distinguishes different stages of coronary artery disease: a cross-sectional study. *Eur Heart J Cardiovasc Imaging* **22**, 298–306 (2021).

204. Diwakar, M. & Kumar, M. A review on CT image noise and its denoising. *Biomedical Signal Processing and Control* vol. 42 Preprint at https://doi.org/10.1016/j.bspc.2018.01.010 (2018).

205. Willemink, M. J. *et al.* Iterative reconstruction techniques for computed tomography Part 1: Technical principles. *Eur Radiol* **23**, (2013).

206. Willemink, M. J. *et al.* Iterative reconstruction techniques for computed tomography part 2: Initial results in dose reduction and image quality. *Eur Radiol* **23**, (2013).

207. Kalender, W. A. X-ray computed tomography. *Physics in Medicine and Biology* vol. 51 Preprint at https://doi.org/10.1088/0031-9155/51/13/R03 (2006).

208. Goldman, L. W. Principles of CT: Radiation dose and image quality. *J Nucl Med Technol* **35**, (2007).

209. Bergström, G. *et al.* The Swedish CArdioPulmonary BioImage Study: objectives and design. *J Intern Med* **278**, 645–659 (2015).

210. Sederberg, T. W. Bezier Curves. *Computer Aided Geometric Design Course Notes* (2012).

211. Breiman, L. Random Forests. *Mach Learn* **45**, 5–32 (2001).

212. Lowe, D. G. Distinctive image features from scale-invariant keypoints. *Int J Comput Vis* **60**, (2004).

213. Nasrudin, M. W. *et al.* Moment Invariants Technique for Image Analysis and Its Applications: A Review. in *Journal of Physics: Conference Series* vol. 1962 (2021).

214. Kolmogorov, V. & Rother, C. Minimizing nonsubmodular functions with graph cuts - A review. *IEEE Transactions on Pattern Analysis and Machine Intelligence* vol. 29 Preprint at https://doi.org/10.1109/TPAMI.2007.1031 (2007).

215. Benčević, M., Galić, I., Habijan, M. & Pižurica, A. Recent Progress in Epicardial and Pericardial Adipose Tissue Segmentation and Quantification Based on Deep Learning: A Systematic Review. *Applied Sciences (Switzerland)* vol. 12 Preprint at https://doi.org/10.3390/app12105217 (2022).

216. Zou, K. H. *et al.* Statistical Validation of Image Segmentation Quality Based on a Spatial Overlap Index. *Acad Radiol* **11**, (2004).

217. Crum, W. R., Camara, O. & Hill, D. L. G. Generalized overlap measures for evaluation and validation in medical image analysis. *IEEE Trans Med Imaging* **25**, (2006).

218. Giavarina, D. Understanding Bland Altman analysis. *Biochem Med (Zagreb)* **25**, (2015).

219. Dey, D. *et al.* Artificial Intelligence in Cardiovascular Imaging: JACC State-of-the-Art Review. *J Am Coll Cardiol* **73**, 1317–1335 (2019).

220. Zhao, Z. Q., Zheng, P., Xu, S. T. & Wu, X. Object Detection with Deep Learning: A Review. *IEEE Transactions on Neural Networks and Learning Systems* vol. 30 Preprint at https://doi.org/10.1109/TNNLS.2018.2876865 (2019).

221. Schmidhuber, J. Deep Learning in neural networks: An overview. *Neural Networks* vol. 61 Preprint at https://doi.org/10.1016/j.neunet.2014.09.003 (2015).

222. Ling, Q. Machine learning algorithms review. *Applied and Computational Engineering* **4**, (2023).

223. Obermeyer, Z. & Emanuel, E. J. Predicting the Future - Big Data, Machine Learning, and Clinical Medicine. *N Engl J Med* **375**, 1216–1219 (2016).

224. Shorten, C. & Khoshgoftaar, T. M. A survey on Image Data Augmentation for Deep Learning. *J Big Data* **6**, (2019).

225. Molnar, D. *et al.* Artificial intelligence based automatic quantification of epicardial adipose tissue suitable for large scale population studies. *Sci Rep* **11**, 23905 (2021).

226. Smirnov, N. Table for Estimating the Goodness of Fit of Empirical Distributions. *The Annals of Mathematical Statistics* **19**, (1948).

227. Massey, F. J. The Kolmogorov-Smirnov Test for Goodness of Fit. *J Am Stat Assoc* **46**, (1951).

228. Gregorutti, B., Michel, B. & Saint-Pierre, P. Correlation and variable importance in random forests. *Stat Comput* **27**, 659–678 (2017).

229. Pearson, K. X. On the criterion that a given system of deviations from the probable in the case of a correlated system of variables is such that it can be reasonably supposed to have arisen from random sampling . *The London, Edinburgh, and Dublin Philosophical Magazine and Journal of Science* **50**, (1900).

230. Kruskal, W. H. & Wallis, W. A. Use of Ranks in One-Criterion Variance Analysis. *J Am Stat Assoc* **47**, (1952).

231. Kendall, M. G. A New Measure of Rank Correlation. *Biometrika* **30**, (1938).

232. Natekin, A. & Knoll, A. Gradient boosting machines, a tutorial. *Front Neurorobot* **7**, (2013).

233. Fawcett, T. An introduction to ROC analysis. *Pattern Recognit Lett* **27**, (2006).

234. Majnik, M. & Bosnić, Z. ROC analysis of classifiers in machine learning: A survey. *Intelligent Data Analysis* vol. 17 Preprint at https://doi.org/10.3233/IDA-130592 (2013).

235. Metz, C. E. ROC analysis in medical imaging: a tutorial review of the literature. *Radiological physics and technology* vol. 1 Preprint at https://doi.org/10.1007/s12194-007-0002-1 (2008).

236. Zhu, Q. On the performance of Matthews correlation coefficient (MCC) for imbalanced dataset. *Pattern Recognit Lett* **136**, (2020).

237. Chicco, D. & Jurman, G. The advantages of the Matthews correlation coefficient (MCC) over F1 score and accuracy in binary classification evaluation. *BMC Genomics* **21**, (2020).

238. Chicco, D., Warrens, M. J. & Jurman, G. The Matthews Correlation Coefficient (MCC) is More Informative Than Cohen's Kappa and Brier Score in Binary Classification Assessment. *IEEE Access* **9**, (2021).

239. Chicco, D. & Jurman, G. The Matthews correlation coefficient (MCC) should replace the ROC AUC as the standard metric for assessing binary classification. *BioData Min* **16**, (2023).

240. Chicco, D., Tötsch, N. & Jurman, G. The matthews correlation coefficient (Mcc) is more reliable than balanced accuracy, bookmaker informedness, and markedness in two-class confusion matrix evaluation. *BioData Min* **14**, (2021).

241. MathWorks, T. MATLAB (R2022a). *The MathWorks Inc.* (2022).

242. IBM® SPSS®. SPSS Software | IBM. *IBM* (2019).

243. R Core Team. The R Project for Statistical Computing, Vienna, Austria. *https://www.R-project.org/* (2020).

244. RStudio Team. RStudio | Open source & professional software for data science teams - RStudio. *RStudio Inc.* (2020).

245. Lin, L. I.-K. A Concordance Correlation Coefficient to Evaluate Reproducibility. *Biometrics* **45**, (1989).

246. Barbosa, J. G., Figueiredo, B., Bettencourt, N. & Tavares, J. M. Towards automatic quantification of the epicardial fat in non-contrasted CT images. *Comput Methods Biomech Biomed Engin* **14**, 905–914 (2011).

247. Marwan, M. & Achenbach, S. Quantification of epicardial fat by computed tomography: why, when and how? *J Cardiovasc Comput Tomogr* **7**, 3–10 (2013).

248. Commandeur, F. *et al.* Fully Automated CT Quantification of Epicardial Adipose Tissue by Deep Learning: A Multicenter Study. *Radiol Artif Intell* **1**, e190045 (2019).

249. Tajbakhsh, N. *et al.* Convolutional Neural Networks for Medical Image Analysis: Full Training or Fine Tuning? *IEEE Trans Med Imaging* **35**, (2016).

250. Mikołajczyk, A. & Grochowski, M. Data augmentation for improving deep learning in image classification problem. in *2018 International Interdisciplinary PhD Workshop, IIPhDW 2018* (2018). doi:10.1109/IIPHDW.2018.8388338.

251. Zhang, L. *et al.* Development of artificial intelligence in epicardial and pericoronary adipose tissue imaging: a systematic review. *Eur J Hybrid Imaging* **5**, 14 (2021).

252. Schofield, R. *et al.* Image reconstruction: Part 1 – understanding filtered back projection, noise and image acquisition. *Journal of Cardiovascular Computed Tomography* vol. 14 Preprint at https://doi.org/10.1016/j.jcct.2019.04.008 (2020).

253. Tayal, U. *et al.* Image reconstruction in cardiovascular CT: Part 2 – Iterative reconstruction; potential and pitfalls. *Journal of Cardiovascular Computed Tomography* vol. 13 Preprint at https://doi.org/10.1016/j.jcct.2019.04.009 (2019).

254. Chun, M., Choi, J. H., Kim, S., Ahn, C. & Kim, J. H. Fully automated image quality evaluation on patient CT: Multi-vendor and multireconstruction study. *PLoS One* **17**, (2022).

255. Song, D. K. *et al.* Increased epicardial adipose tissue thickness in type 2 diabetes mellitus and Obesity. *Diabetes Metab J* **39**, (2015).

256. Demircelik, M. B. *et al.* Epicardial adipose tissue and pericoronary fat thickness measured with 64-multidetector computed tomography:

Potential predictors of the severity of coronary artery disease. *Clinics* **69**, (2014).

257. McClain, J. *et al.* Pericardial adipose tissue and coronary artery calcification in the Multi-ethnic Study of Atherosclerosis (MESA). *Obesity* **21**, (2013).

258. Ding, J. *et al.* The association of pericardial fat with calcified coronary plaque. *Obesity* **16**, (2008).

259. Commandeur, F. *et al.* Deep Learning for Quantification of Epicardial and Thoracic Adipose Tissue From Non-Contrast CT. *IEEE Trans Med Imaging* **37**, 1835–1846 (2018).

260. McCollough, C. H. *et al.* Coronary artery calcium: a multi-institutional, multimanufacturer international standard for quantification at cardiac CT. *Radiology* **243**, 527–538 (2007).

261. Hindso, L., Jakobsen, L. S., Jacobsen, C., Lynnerup, N. & Banner, J. Epicardial adipose tissue volume estimation by postmortem computed tomography of eviscerated hearts. *Forensic Sci Med Pathol* **13**, 468–472 (2017).

262. So, A. & Nicolaou, S. Spectral computed tomography: Fundamental principles and recent developments. *Korean Journal of Radiology* vol. 22 Preprint at https://doi.org/10.3348/kjr.2020.0144 (2021).

263. Etter, D. *et al.* Towards universal comparability of pericoronary adipose tissue attenuation: a coronary computed tomography angiography phantom study. *Eur Radiol* **33**, (2023).

264. Zheng, X. *et al.* Body size and tube voltage dependent corrections for Hounsfield Unit in medical X-ray computed tomography: theory and experiments. *Sci Rep* **10**, (2020).

265. Goeller, M. *et al.* Pericoronary adipose tissue CT attenuation and its association with serum levels of atherosclerosis-relevant inflammatory mediators, coronary calcification and major adverse cardiac events. *J Cardiovasc Comput Tomogr* **15**, (2021).

266. Elnabawi, Y. A. *et al.* Association of Biologic Therapy with Coronary Inflammation in Patients with Psoriasis as Assessed by Perivascular Fat Attenuation Index. *JAMA Cardiol* **4**, (2019).

267. Kwiecinski, J. *et al.* Peri-Coronary Adipose Tissue Density Is Associated With 18F-Sodium Fluoride Coronary Uptake in Stable Patients With High-Risk Plaques. *JACC Cardiovasc Imaging* **12**, (2019).

268. El Khoudary, S. R. *et al.* Effects of hormone therapy on heart fat and atherosclerosis progression in recently postmenopausal women from keeps trial. *Menopause* **25**, (2018).

269. Cabrera-Rego, J. O. *et al.* Association between endothelial dysfunction, epicardial fat and subclinical atherosclerosis during menopause. *Clinica e Investigacion en Arteriosclerosis* **30**, (2018).

270. Zhao, E. *et al.* Branched-Chain Amino Acids in Computed Tomography– Defined Adipose Depots and Coronary Artery Disease: A PROMISE Trial Biomarker Substudy. *J Am Heart Assoc* **12**, (2023).

271. Foldyna, B. *et al.* Epicardial Adipose Tissue in Patients With Stable Chest Pain: Insights From the PROMISE Trial. *JACC: Cardiovascular Imaging* vol. 13 Preprint at https://doi.org/10.1016/j.jcmg.2020.05.024 (2020).

272. Hsieh, J. & Flohr, T. Computed tomography recent history and future perspectives. *Journal of Medical Imaging* **8**, (2021).

273. Kuneman, J. H. *et al.* Pericoronary Adipose Tissue Attenuation in Patients with Acute Coronary Syndrome Versus Stable Coronary Artery Disease. *Circ Cardiovasc Imaging* **16**, (2023).

274. Ichikawa, K. *et al.* High pericoronary adipose tissue attenuation on computed tomography angiography predicts cardiovascular events in patients with type 2 diabetes mellitus: post-hoc analysis from a prospective cohort study. *Cardiovasc Diabetol* **21**, (2022).

275. Goeller, M. *et al.* Relationship between changes in pericoronary adipose tissue attenuation and coronary plaque burden quantified from

coronary computed tomography angiography. *Eur Heart J Cardiovasc Imaging* **20**, (2019).

276. Kanaji, Y. *et al.* Pre-percutaneous coronary intervention pericoronary adipose tissue attenuation evaluated by computed tomography predicts global coronary flow reserve after urgent revascularization in patients with non–st-segment–elevation acute coronary syndrome. *J Am Heart Assoc* **9**, (2020).

277. Tzolos, E. *et al.* Pericoronary Adipose Tissue Attenuation, Low-Attenuation Plaque Burden, and 5-Year Risk of Myocardial Infarction. *JACC Cardiovasc Imaging* **15**, (2022).

278. Sun, J. T. *et al.* Pericoronary Fat Attenuation Index Is Associated With Vulnerable Plaque Components and Local Immune-Inflammatory Activation in Patients With Non-ST Elevation Acute Coronary Syndrome. *J Am Heart Assoc* **11**, (2022).

279. Lin, A., Dey, D., Wong, D. T. L. & Nerlekar, N. Perivascular Adipose Tissue and Coronary Atherosclerosis: from Biology to Imaging Phenotyping. *Current Atherosclerosis Reports* vol. 21 Preprint at https://doi.org/10.1007/s11883-019-0817-3 (2019).

280. Sagris, M. *et al.* Pericoronary fat attenuation index—a new imaging biomarker and its diagnostic and prognostic utility: a systematic review and meta-analysis. *European Heart Journal Cardiovascular Imaging* vol. 23 Preprint at https://doi.org/10.1093/ehjci/jeac174 (2022).

281. Hell, M. M. *et al.* CT-based analysis of pericoronary adipose tissue density: Relation to cardiovascular risk factors and epicardial adipose tissue volume. *J Cardiovasc Comput Tomogr* **10**, (2016).

282. van Rosendael, S. E. *et al.* Vessel and sex differences in pericoronary adipose tissue attenuation obtained with coronary CT in individuals without coronary atherosclerosis. *International Journal of Cardiovascular Imaging* (2022) doi:10.1007/s10554-022-02716-7.

283. Balcer, B. *et al.* Pericoronary fat volume but not attenuation differentiates culprit lesions in patients with myocardial infarction. *Atherosclerosis* **276**, (2018).

284. Budoff, M. J. & Gul, K. M. Expert review on coronary calcium. *Vascular Health and Risk Management* vol. 4 Preprint at https://doi.org/10.2147/vhrm.s1160 (2008).

285. Wexler, L. *et al.* Coronary artery calcification: Pathophysiology, epidemiology, imaging methods, and clinical implications. A statement for health professionals from the American Heart Association. *Circulation* vol. 94 Preprint at https://doi.org/10.1161/01.CIR.94.5.1175 (1996).

286. de Vos, B. D. *et al.* Direct Automatic Coronary Calcium Scoring in Cardiac and Chest CT. *IEEE Trans Med Imaging* **38**, (2019).

287. Lessmann, N. *et al.* Deep convolutional neural networks for automatic coronary calcium scoring in a screening study with low-dose chest CT. in *Medical Imaging 2016: Computer-Aided Diagnosis* vol. 9785 (2016).

288. Sandstedt, M. *et al.* Evaluation of an AI-based, automatic coronary artery calcium scoring software. *Eur Radiol* **30**, 1671–1678 (2020).

289. Wexler, L. *et al.* Coronary Artery Calcification: Pathophysiology, Epidemiology, Imaging Methods, and Clinical Implications. *Circulation* **94**, (1996).

290. Sage, A. P., Tintut, Y. & Demer, L. L. Regulatory mechanisms in vascular calcification. *Nature Reviews Cardiology* vol. 7 Preprint at https://doi.org/10.1038/nrcardio.2010.115 (2010).

291. Durham, A. L., Speer, M. Y., Scatena, M., Giachelli, C. M. & Shanahan, C. M. Role of smooth muscle cells in vascular calcification: Implications in atherosclerosis and arterial stiffness. *Cardiovascular Research* vol. 114 Preprint at https://doi.org/10.1093/cvr/cvy010 (2018).

292. Bentzon, J. F., Otsuka, F., Virmani, R. & Falk, E. Mechanisms of plaque formation and rupture. *Circ Res* **114**, (2014).

293. Eckel, R. H., Bornfeldt, K. E. & Goldberg, I. J. Cardiovascular disease in diabetes, beyond glucose. *Cell Metabolism* vol. 33 Preprint at https://doi.org/10.1016/j.cmet.2021.07.001 (2021).

294. Galicia-Garcia, U. *et al.* Pathophysiology of type 2 diabetes mellitus. *International Journal of Molecular Sciences* vol. 21 Preprint at https://doi.org/10.3390/ijms21176275 (2020).

295. Einarson, T. R., Acs, A., Ludwig, C. & Panton, U. H. Prevalence of cardiovascular disease in type 2 diabetes: A systematic literature review of scientific evidence from across the world in 2007-2017. *Cardiovascular Diabetology* vol. 17 Preprint at https://doi.org/10.1186/s12933-018-0728-6 (2018).

296. Poznyak, A. *et al.* The diabetes mellitus–atherosclerosis connection: The role of lipid and glucose metabolism and chronic inflammation. *International Journal of Molecular Sciences* vol. 21 Preprint at https://doi.org/10.3390/ijms21051835 (2020).

297. Ernault, A. C., Meijborg, V. M. F. & Coronel, R. Modulation of Cardiac Arrhythmogenesis by Epicardial Adipose Tissue: JACC State-of-the-Art Review. *Journal of the American College of Cardiology* vol. 78 Preprint at https://doi.org/10.1016/j.jacc.2021.08.037 (2021).

298. Wong, C. X. *et al.* Associations of Epicardial, Abdominal, and Overall Adiposity with Atrial Fibrillation. *Circ Arrhythm Electrophysiol* **9**, (2016).

299. Al Chekakie, M. O. *et al.* Pericardial fat is independently associated with human atrial fibrillation. *J Am Coll Cardiol* **56**, (2010).

300. Patel, K. H. K., Hwang, T., Liebers, C. S. & Ng, F. S. Epicardial adipose tissue as a mediator of cardiac arrhythmias. *American Journal of Physiology - Heart and Circulatory Physiology* vol. 322 Preprint at https://doi.org/10.1152/ajpheart.00565.2021 (2022).

301. Lau, D. H., Linz, D. & Sanders, P. New Findings in Atrial Fibrillation Mechanisms. *Cardiac Electrophysiology Clinics* vol. 11 Preprint at https://doi.org/10.1016/j.ccep.2019.08.007 (2019).

302. Conte, M. *et al.* Epicardial Adipose Tissue and Cardiac Arrhythmias: Focus on Atrial Fibrillation. *Frontiers in Cardiovascular Medicine* vol. 9 Preprint at https://doi.org/10.3389/fcvm.2022.932262 (2022).

303. Zhou, M., Wang, H., Chen, J. & Zhao, L. Epicardial adipose tissue and atrial fibrillation: Possible mechanisms, potential therapies, and future directions. *PACE - Pacing and Clinical Electrophysiology* vol. 43 Preprint at https://doi.org/10.1111/pace.13825 (2020).